MODERN XRD METHODS IN MINERALOGY

Robert E. Dinnebier & Karen Friese, Max-Planck-Institute for Solid State Research, Stuttgart. FRG

Keywords
Powder diffraction, single crystal diffraction, synchrotron radiation, neutron radiation, diffractometer, structure determination, structure refinement.

Contents

Glossary

Absorption: Decrease of intensity of electromagnetic waves while traveling through matter due to excitation of the absorbing material
Absorption edge: Frequency of a sudden increase in the absorption spectra of an element due to the fact that the incoming energy is exactly equal to the energy for excitation or ionization. The scattering close to an absorption edge is called anomalous scattering.
Atomic form factor: Scattering power of an isolated atom as a function of scattering angle.
Bragg-Brentano geometry: Geometry of an instrumental setup for powder diffraction in reflection mode with variable radius of the focusing circle.
Bragg equation: Equation describing the condition for X-ray diffraction by crystalline solids.
Crystallite size: macroscopic dimension of a crystalline grain.
Darwin width: Smallest possible width at half maximum of a diffraction peak of an ideal crystal according to the laws of diffraction physics.
Debye-Scherrer cone: Diffraction cone of a powder of randomly oriented crystallites with opening angle 4Θ.
Debye-Scherrer method: non-focusing powder method in transmission mode where the diffraction cones are recorded equatorially on a cylinder by film or other media.
Diamond anvil cell (DAC): High pressure cell where the pressure is generated between the culets of diamonds.
Diffraction: Deviation of a wave from the incoming direction due to an obstacle; always accompanied by constructive or destructive interference.
Diffractometer: Device for the measurement of diffracted intensities from a monocrystalline or polycrystalline sample.
Direct lattice: Lattice used to describe the arrangement of atoms in a crystalline solid; defined by six basis parameters $(a, b, c, \alpha, \beta, \gamma)$.
Direct methods: Method for structure determination which reconstructs the phases of the reflections by statistical means using the relationship between normalized structure factors.
Displacement factor: Factor describing the deviation of the atoms from the ideal position in a lattice (due to e.g. thermal motion).
Domain: Region of a crystal in which an individual vector quantity has the same value.
d-spacing: Distance between the lattice planes of a crystal.
Electron density: Distribution of electrons within a unit cell.
Extinction conditions: Conditions describing the systematic absence of reflections in reciprocal space due to the existence of lattice centering, glide planes or screw axis.
Ewald sphere: Graphical aid for visualization of the diffraction condition.
Full width at half maximum (FWHM): Breadth of a peak at half of its height.
Global optimization methods: Real space methods for structure determination like e.g. the method of simulated annealing.
Least Squares methods: Mathematical method for the minimization of the squared differences between observed and calculated quantities.
LeBail method: Method for profile refinement and intensity extraction of powder diffraction data using the Rietveld decomposition formula starting from uniform peak intensities.
Miller indices hkl: Integers describing the orientation of a lattice plane, based on the reciprocal ratio of the interceptions of the axes.
Mineral: Homogeneous, inorganic crystalline solid of natural origin.
Monochromatic radiation: Radiation of an ideally infinitely small wavelength band.
Mosaic block: Coherent scattering part of a single crystal with ideal periodicity.
Neutron diffraction: Diffraction method based on the scattering of neutrons by matter.
Pawley method: Method for profile refinement and intensity extraction of powder diffraction data constrained only by lattice parameters and FWHM distribution.

Peak profile function: Mathematical function (e.g. Gauss or Lorentz distribution) describing the shape of a peak.

Phase problem in crystallography: How to identify the atomic positions starting only from the modulo of the structure factor.

Point group: Mathematical group with translations, rotations and roto-inversions as symmetry operators used to describe the symmetry in crystallography.

Reciprocal lattice: Mathematical construction useful in diffraction physics, where the reciprocal basis vectors satisfy the following conditions $a^*=(b\times c)/V$, $b^*=(c\times a)/V$, $c^*=(a\times b)/V$ (see nomenclature).

Rietveld refinement: Least squares method for profile and crystal structure refinement of powder diffraction data based on the entire powder pattern.

Crystal: An ideal crystal consists of an infinite three-dimensional periodic arrangement of atoms. In real crystals, the periodicity is generally disturbed by the formation of mosaic blocks or domains.

Space groups: 230 mathematical groups describing the symmetry of a crystal structure in three dimensions.

Strain: Deformation of a material in space in accordance to its elastic constants caused by internal or external stress.

Structure factor F_{hkl}: Sum of the scattered waves of all atoms in the unit cell in direction of hkl. The modulo is equal to the square root of the intensity I_{hkl}, whereas the phase is determined by the position of the atoms.

Synchrotron radiation: Radiation emitted during acceleration of charged particles which move at a velocity close to that of light.

Texture: Anisotropic intensity distribution caused by the orientations of crystallites in polycrystalline material.

Unit cell: Basic unit in a crystal lattice, defined by three linearly independent basic vectors; the whole crystal is build up from the unit cell by applying translational symmetry operations.

Wavelength: Minimal distance between two points with identical phase in a wave.

X-ray: Electromagnetic radiation with a wavelength in the range of 10^{-5} – 100Å.

Nomenclature

a, b, c	basis vectors in direct space
a^*, b^*, c^*	basis vectors in reciprocal space
$A_{pH}(2\Theta_i)$	absorption correction of phase P and reflection H in a Rietveld refinement
α, β, γ	angles between the basis vectors in direct space.
$\alpha^*, \beta^*, \gamma^*$	angles between the basis vectors in reciprocal space.
B_j	isotropic displacement factor of atom j
B	background of reflection
$B_i(obs)$	background contribution at step i in a powder pattern
β_{hkl}	FWHM (full width half maximum) in radians
c	velocity of light
d	interplanar lattice spacing
d^*	reciprocal lattice spacing
e	charge of electron
E	energy
f_0	atomic form factor at T= 0 K
f', f''	real and imaginary parts of the anomalous dispersion correction of the atomic form factor
E_{hkl} , E_H	normalized structure factor
F_{hkl}, F_H	structure factor for reflection hkl (H)

ε	dilation $\Delta d/d$ (strain)
F_o, F_c	observed and calculated structure factor for reflection hkl (H)
FWHM	full width half maximum
$F(2\Theta)$	profile function of a powder diffraction peak
G	instrumental broadening function
φ	diffractometer angle
φ_a, φ_b, φ_c	angles between diffracted beam and basis vectors
φ_a^0, φ_b^0, φ_c^0	angles between primary beam and basis vectors
$\phi_{pH}(2\Theta_i)$	normalized powder peak profile function of phase p and reflection H
Γ	peak broadening (FHWM) of a powder peak
Γ_A	anisotropic strain contribution to the peak broadening
Γ_G, Γ_L	Gauss- and Lorentz part of the FWHM distribution
h	Planck’s constant
h, k, l	Miller indices
H	lattice point in reciprocal space
I	integrated intensity
κ	diffractometer angle (kappa geometry)
$LP(2\Theta_i)$	Lorentz Polarization correction
L_{hkl}	average grain size
λ	wavelength
M, M_{pH}	multiplicity (of phase P and reflection H in a Rietveld refinement)
μ_p	angle between precession axis and primary beam in precession geometry
μ	linear absorption coefficient
ω	diffractometer angle
P(r)	Patterson function
P_{pH}	preferred orientation correction for phase P and reflection H in a Rietveld refinement
ψ	lattice plane
r=xa+yb+zc	position in unit cell
$\rho(r)$, $\rho(x,y,z)$	electronic density function
r^*_H	vector defining a lattice point in reciprocal space
R	agreement factor of a least squares refinement
S_{hkl}	refinable parameters describing the anisotropic peak broadening due to lattice strain in a powder pattern
S_p	scale factor of phase p in a Rietveld refinement
Σ_1, Σ_2 –relationship	relationships used for phasing in direct methods
T_{hkl}	Debye-Waller factor
Θ	Bragg angle
2Θ	diffractometer angle
Θ_m	Bragg angle of monochromator
U, V, W	parameters of the Gauss part of the FWHM
V	volume of the unit cell in direct space
V*	volume of the unit cell in reciprocal space
V	voltage
W	spectral distribution of X-ray radiation
χ	diffractometer angle (Euler geometry)
X, Y	parameters of the Lorentz part of the FWHM
x, y, z	fractional coordinates of atoms
y_i (calc)	calculated intensity at position i in a powder pattern
Z	atomic number

ζ	mixing parameter describing the fraction of the Gauss part of the FWHM distribution to the anisotropic strain broadening

Summary

The following article describes the basics of crystal structure determination and refinement from X-ray diffraction data with focus on applications in mineralogy.

1 Introduction

Since the performance of the first X-ray diffraction experiments on a single crystal in 1912, X-ray crystallography has been of major importance in natural sciences and especially in mineralogy. X-ray diffraction provided the ideal means to understand structures of minerals (and other crystalline matter) on an atomic scale. It thus established relationships between the crystal structure and the physical and chemical properties of the material under investigation. In other cases it related the crystal structure to the special thermodynamical conditions under which a mineral (or a rock) has been formed and thus provided important information for petrology and geology. In particular the powder diffraction method allowed the unambiguous identification of minerals and –with the introduction of quantitative phase analysis – also the quantification of the different phases of a mixture, e.g. a rock.

The structure determination of minerals exhibits several typical difficulties. Often the chemical composition is quite variable, requiring a distinct contrast in scattering power of the different elements to allow for successful identification. Two (or more) chemical elements can occupy the same crystallographic site. This frequently leads to different degrees of long and short range ordering, which often implies the existence of very weak intensities or diffuse scattering, making X-ray crystallography on minerals far more challenging than crystallography on synthetic materials. This is especially true for the wide range of alumosilicates which include most of the rock-forming minerals.

With the availability of neutron and synchrotron radiation sources, new fields of research were developed: The entirely different dependence of the scattering power on the order number of the elements for neutron- compared to X-ray diffraction, allows to distinguish between neighboring elements in the periodic table. Furthermore, neutron diffraction provides the means to determine magnetic structures. On the other hand, the high brilliance, low divergence, and wavelength tunability of synchrotron radiation is of crucial importance for the detection of weak intensities, the measurement of crystals with very large unit cell, and it allows to make use of the effect of anomalous dispersion. In any case, the strongest impact is observed in the field of powder diffraction, where the two new sources enhance the resolution of a powder diffraction pattern by more than an order of magnitude compared to laboratory sources. Consequently, more complicated crystal structures can be solved with increasing accuracy by the powder method. Additionally the higher resolution allows extraction of detailed microstructural information on e.g. lattice strain or domain size.

This compact review on modern X-ray crystallography in mineralogy gives a basic introduction to the different methods and their applications. Both single crystal and X-ray powder diffraction procedures are included, with an emphasis on modern powder diffraction using synchrotron radiation. Wherever possible focus is on applications directly related to mineralogical problems.

Due to the restricted space for literature references only the most helpful sources used for the preparation of this review have been cited.

2 The diffraction of X-rays

In the year 1912, Friedrich, Knipping and von Laue performed the first diffraction experiment using single crystals of copper sulfate and zinc sulfite. Based on these experiments Max von Laue developed his theory of X-ray diffraction. At the same time W. L. Bragg and W. H. Bragg performed their diffraction experiments and in turn used an alternative though equivalent way of explaining the observed diffraction phenomena. Up to now the so-called Laue conditions and the Bragg equation are the basis of X-ray diffraction of crystalline material and it is therefore inevitable to start any monograph on X-ray crystallography with a short resume of the investigations carried out by these scientists.

Like visible light an X-ray beam is an electromagnetic wave characterized by an electric field vector *E* which is perpendicular to the direction of propagation and a magnetic field vector *H* which in turn is perpendicular both to *E* and the direction of propagation. Yet compared to an optical wave the wavelength of an X-ray beam is considerably shorter: thus the spectra of visible light comprises the range from 4000 to 7000 Å, while X-rays have typically wavelengths between 0.1 to 10 Å. Due to the fact that X-ray wavelengths are comparable to the interatomic distances within a crystalline material one observes characteristic interactions between the X-rays and the ordered array of electrons in the crystal structure. These interactions make X-rays the most important source for the investigation of crystal structures. The nature of these interactions as well as the basic laws of diffraction will be explained in this chapter.

If the electromagnetic X-ray waves encounter an object, they are scattered by the electrons of the object. The field of the X-rays forces the electrons within the material to oscillate and the electrons are in turn the starting point of secondary waves of the same frequency and wavelength like the primary waves. These waves superimpose and if constructive interference occurs give rise to the different diffraction phenomena which are generally strong if the distances within the object are comparable to the wavelength of the incoming beam. In addition the periodic nature of the atomic arrangement within a crystal gives rise to special diffraction phenomena which are in many ways comparable to the diffraction of visible light by a refraction lattice.

2.1 The Laue equations

To understand diffraction in a three dimensional crystal it is helpful to concentrate on the one-dimensional case first. Figure 1 shows a one dimensional lattice which consists of a row of pointlike scattering centers, which are separated by a periodic distance *a*. If a plane wave hits such a row of points every scatterer gives rise to a new secondary wave, which propagates in a spherical manner. The individual scattered waves superimpose and generally extinguish each other. Only along the common tangents will the spherical waves oscillate with identical phases and therefore interfere in a constructive way forming a common **diffracted** wave. It can be seen in the figure that the planes of common tangents exist in various directions, which define the different diffraction orders.

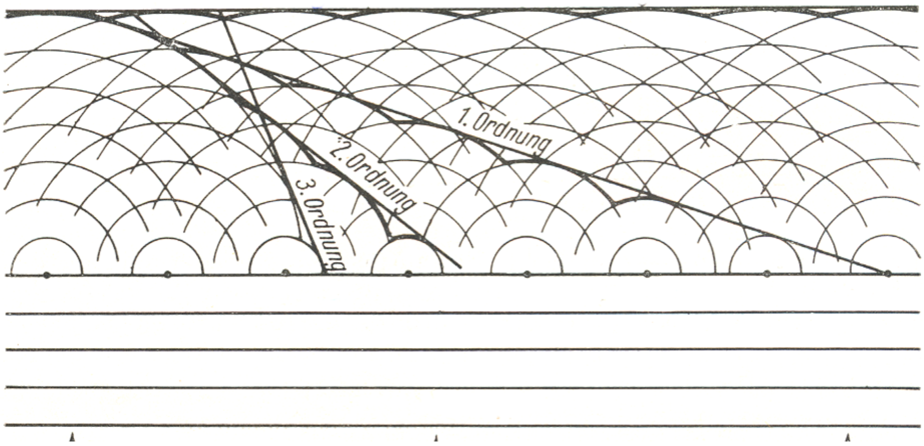

Figure 1: Diffraction of a plane wave by a row of pointlike scatterers

The diffracted waves of all orders have the same wavelength as the incoming primary beam. If one completes the figure in the third direction perpendicular to the plane of paper, it becomes evident that the resulting wavefront moves along a cone.

Figure 2 shows the same conditions but now the direction of the primary beam forms an arbitrary angle $\varphi_a{}^0$ with the diffracting array of points. The cone-like wavefront of first order is shown. The diffracted beams which are perpendicular to this wavefront form in turn a cone with an opening angle of $2\varphi_a$. The phase difference between two waves which have been diffracted by neighboring points is - in the case of the first diffraction order - exactly equal to the wavelength λ: Following the figure one can see that the phase difference is given by:

$$s - t = a\cos\varphi_a - a\cos\varphi_a^0 = a(\cos\varphi_a - \cos\varphi_a^0) = \lambda \tag{1}$$

and for the second order

$$s - t = a\cos\varphi_a - a\cos\varphi_a^0 = a(\cos\varphi_a - \cos\varphi_a^0) = 2\lambda \tag{2}$$

or generally

$$s - t = a\cos\varphi_a - a\cos\varphi_a^0 = a(\cos\varphi_a - \cos\varphi_a^0) = h\lambda \tag{3}$$

where *h* is an integer. Considering now a three dimensional lattice it is evident that every lattice direction requires a similar condition. For the lattice vectors in the direction of the three lattice parameters *a*, *b*, *c* these conditions are:

$$\begin{aligned} a(\cos\varphi_a - \cos\varphi_a^0) &= h\lambda \\ b(\cos\varphi_b - \cos\varphi_b^0) &= k\lambda \\ c(\cos\varphi_c - \cos\varphi_c^0) &= l\lambda \end{aligned} \tag{4}$$

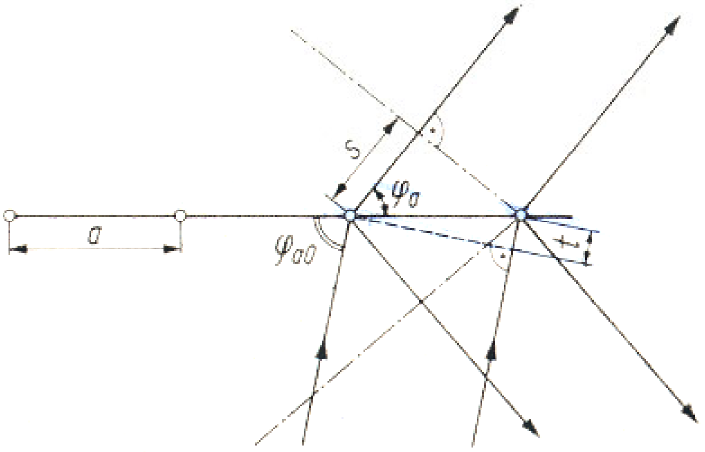

Figure2: Diffraction of a plane wave by a row of pointlike scatterers

These equations are called the **Laue equations.** φ_a^0, φ_b^0 and φ_c^0 are the angles between the incoming primary beam and the three basis vectors while φ_a, φ_b and φ_c are the angles between the basis vectors and the diffracted secondary beam; *h*, *k*, *l* are integers. The equations for all other lattice directions are linear combinations from the above three and accordingly no further conditions have to be defined.

Diffraction from a three dimensional lattice can only exist if the conditions (1) are simultaneously fulfilled for all three directions. Whenever the condition is fulfilled for the direction of a basis vector a cone of diffracted beams is formed which opens in the direction of the corresponding vector. For two of these cones which open in different directions a common beam only exists in the direction of their mutual intersection. In figure 3 for example the cone formed around the vector *a* and the second cone formed around the vector *b* have a common beam in the direction of *k*. A third cone, which opens around the vector *c* does not intersect with the former two and does not contain the direction *k*. This proves that not all the three Laue conditions are fulfilled at the same time and consequently there is no constructive interference between the three beams. If well defined relationships between the lattice vectors, the primary beam direction and the wavelength λ exist, a common direction *k* for the three cones of diffracted beams is observed. Only then the three Laue equations are simultaneously fulfilled and constructive interference of the diffracted waves occurs.

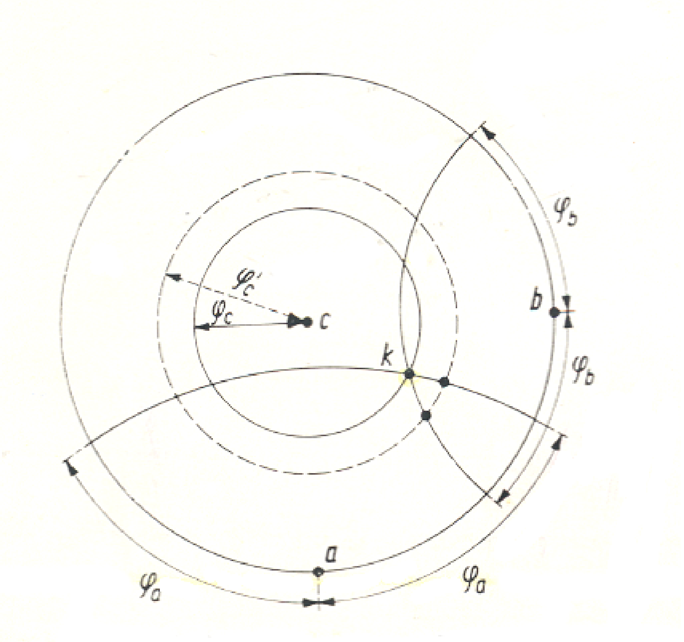

Figure 3: Representation of the Laue conditions for the diffraction by a crystal lattice

2.2 The Bragg equation

An alternative description for the diffraction of X-rays by a lattice plane was suggested by W. L. Bragg in 1912 and is known as the **Bragg-equation**:

$$n \cdot \lambda = 2 \cdot d \cdot \sin(\Theta) \qquad (5)$$

with λ as the wavelengths of the X-rays, d as the interplanar spacing of parallel lattice planes, and 2Θ as the diffraction angle. Figure 4 illustrates this relationship.

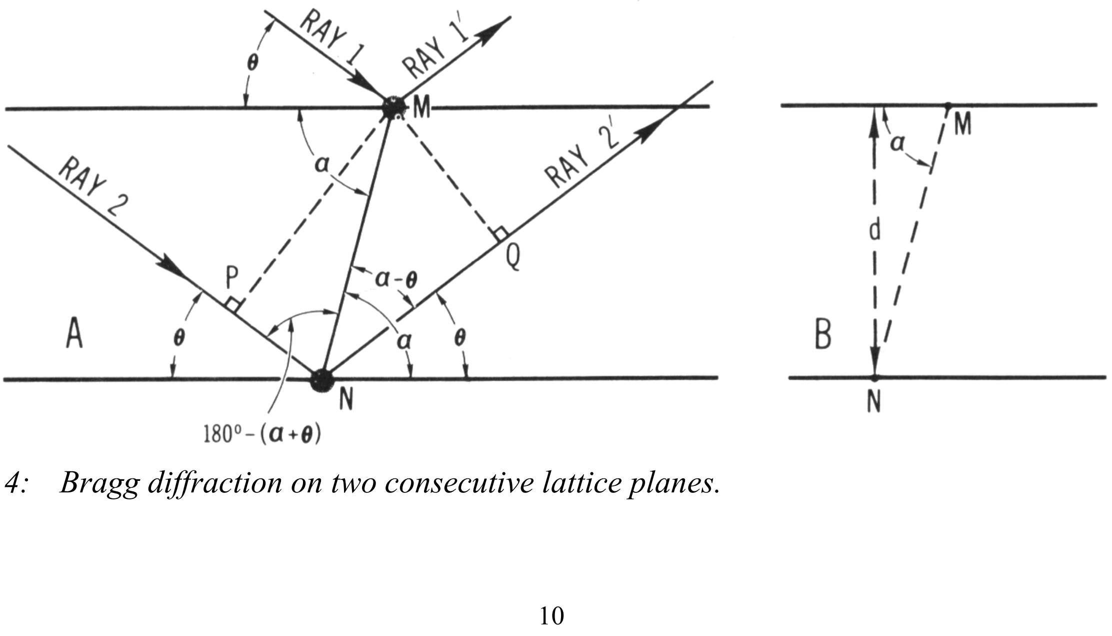

Figure 4: Bragg diffraction on two consecutive lattice planes.

As mentioned above the X-rays will be diffracted by the electrons of the atoms which act as scattering centers by sending out spherical waves. Equation 5 defines in which directions (2Θ), at a fixed value of λ and *d*, constructive interference of the scattered waves is possible.
This is exactly the case if the extra distance traveled by ray 2 in figure 4 is a multiple (*n*) of the wavelength. For simplicity, the number *n* may be included in the indexing of the set of lattice planes ((222)= 2*(111)) and consequently in the *d*-spacing.

Several relationships in crystallography directly follow from the Bragg equation (Eq. 5). It can be shown e.g. that a constant error in 2Θ has a much stronger impact on the error in *d*-spacing at low scattering angles than it has at high angles. Another consequence of the Bragg equation is that the resolution augments with increasing scattering angles. Relationships for strain and domain size can also be derived.

2.3 The Ewald sphere

The so-called Ewald construction or **Ewald sphere** is a useful tool to examine whether the diffraction condition for a reciprocal lattice point (see chapter 6) is fulfilled or not and is widely used in crystallography. Therefore the principle will be briefly outlined here.
We imagine a sphere of radius 1/λ with the primary beam passing through the diameter IO (see Figure 5). The origin of the reciprocal lattice coincides with the point O. If the vector r^*_H lies on the surface of the sphere the corresponding lattice planes *hkl* lie parallel to IP and form an angle θ with the primary beam. Now, the necessary condition to fulfill the Bragg equation is that the lattice point defined by the vector r^*_H (which corresponds to the lattice planes *hkl*) must lie on the surface of the sphere with radius 1/λ which is called the Ewald sphere.

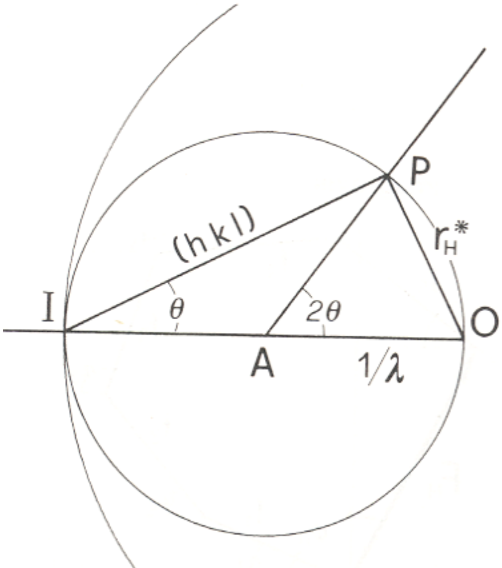

Figure 5 : The Ewald sphere and the limiting sphere (in two dimensions)

For X-rays and neutrons with wavelengths between 0.5 - 2Å the Ewald sphere has an appreciable curvature with respect to the lattice planes. If a monochromatic primary beam and a crystal in arbitrary orientation is used generally none of the reciprocal lattice points touches the surface of the Ewald sphere (excluding the origin of reciprocal space). Therefore, the different experimental techniques described below all try to bring as many reciprocal lattice points as possible onto the surface of the sphere (i. e. into diffraction position).

If $r^*_H > 2/\lambda$ it is not possible to observe the corresponding reflection H. This condition defines the **limiting sphere** with the center O and the radius $2/\lambda$. Only lattice points within the limiting sphere can be brought into diffraction position (this has consequences for the choice of the wavelength in a given experimental setup). On the other hand if $\lambda > 2a_{max}$ (where a_{max} is the largest period of the unit cell) then the diameter of the Ewald sphere is smaller than r^*_{min} (the smallest period of the reciprocal lattice) and no lattice node can intercept the surface of the Ewald sphere.

3 The Generation of the primary beam

In a conventional X-ray laboratory the X-ray beam is generated within a so-called X-ray tube, a schematic representation of which is given in Figure 6. The tube basically consists of two parts: the filament A and the water cooled target material B. Between filament and target a large voltage difference (20,000 to 50,000V) is produced, while the filament is operated by a small voltage of approximately 6-20V. This is sufficient to generate electrons from the filament by thermoionic emission. The huge voltage difference between filament and target material accelerates the generated electrons in the direction of the target material. When some of the accelerated electrons hit the target material they are stopped abruptly and emit in turn an electromagnetic wave. The higher the voltage of the filament the more intense are the X-rays generated. The shortest wavelength λ_0 of these waves is given by the relationship

$$\lambda_0 = hc/Ve \qquad (6)$$

where V is the voltage drop from filament to target, e is the charge of the electron, h is Planck‘s constant and c is the velocity of light. Not all electrons are stopped directly but some have multiple collisions with the target and this multiple stoppage leads to a generation of further electromagnetic waves of increasing wavelengths.

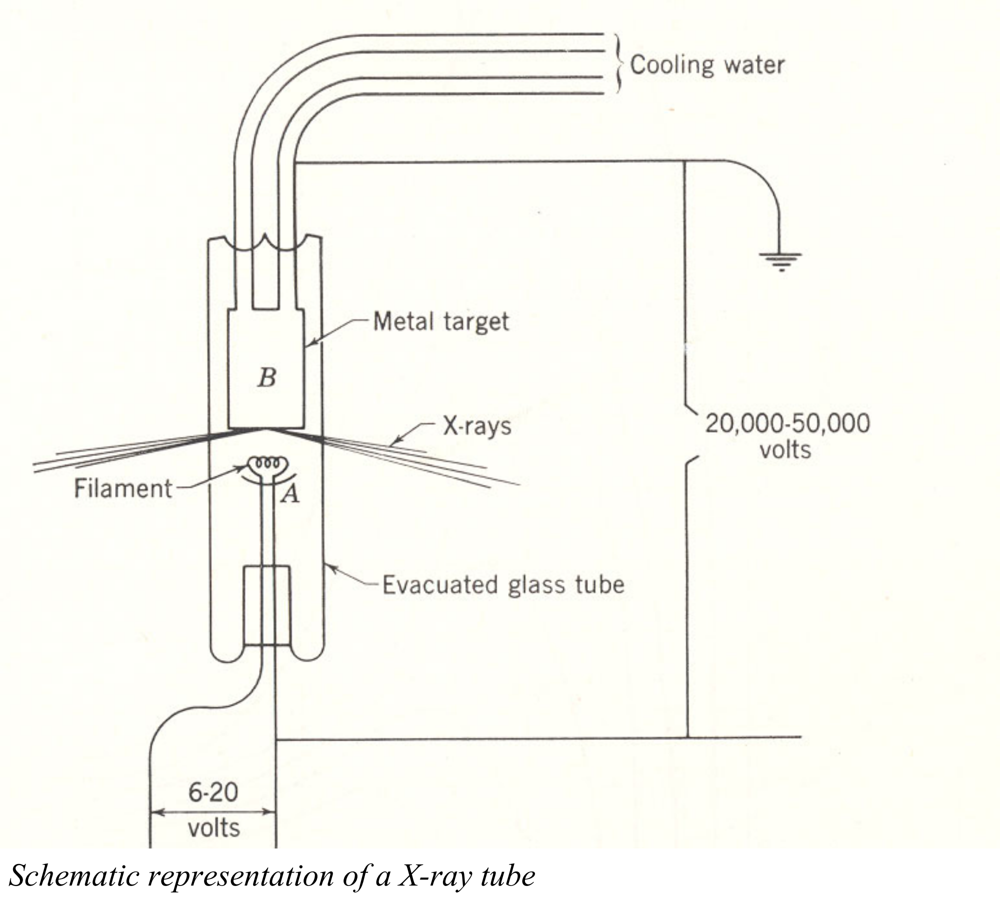

Figure 6: Schematic representation of a X-ray tube

The radiation which is produced due to the stoppage of the electrons from the filament is independent of the target material and is called „continuous radiation“. Yet above this continuous spectrum of wavelengths intense peaks appear which are due to processes in the target material and characteristic for the material used (see figure 7). This radiation is consequently called „characteristic radiation“. Its generation is best understood if one recalls that an atom is composed of a nucleus and various energy levels K, L, M, N in which the electrons are accommodated. If an electron within the target material drops for example from an energy level L to an energy level K (i.e. a level closer to the nucleus) due to the interaction with the accelerated electrons from the filament, it emits energy as radiation. In this special case ($K \rightarrow L$) this radiation is called K_α radiation. If the electron drops from the energy level M to level K the so-called K_β radiation is emitted.

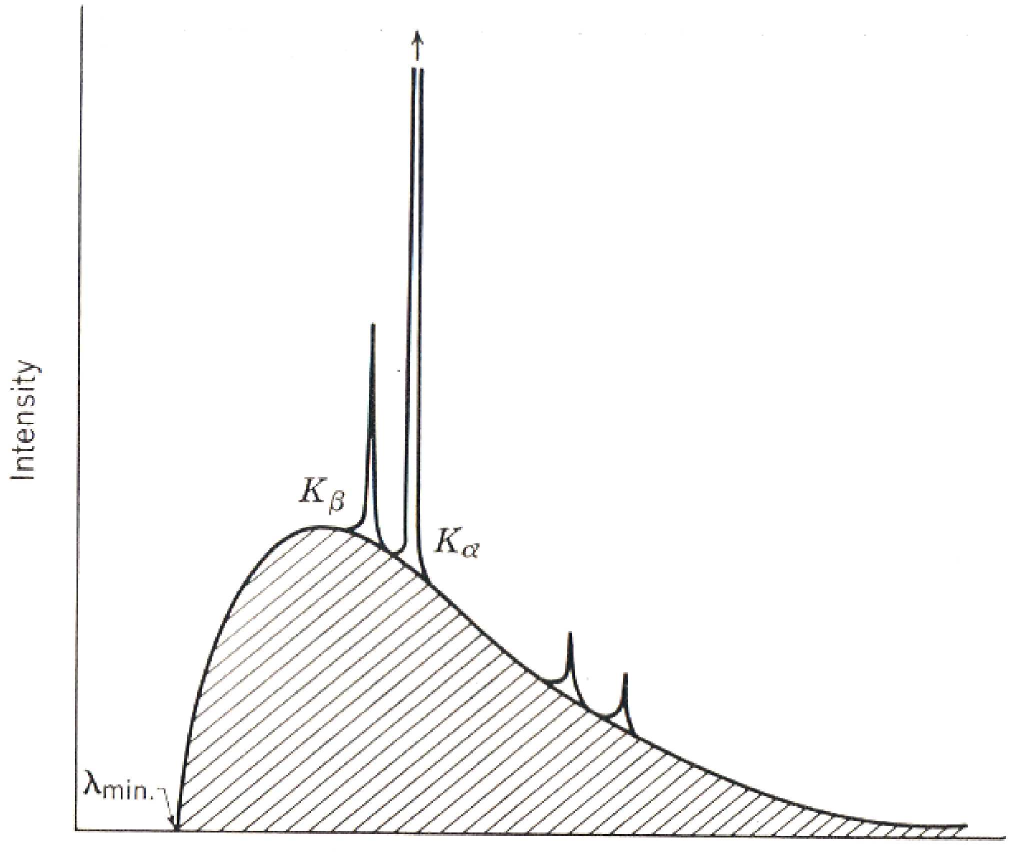

Figure 7: The characteristic and continuous radiation as emitted by an X-ray tube

Apart from X-rays two other types of radiation are important in crystallography, synchrotron and neutron radiation. The generation of the primary beam for these two radiation sources will be briefly explained now.

Electronically charged particles which move within an accelerator ring with velocities close to that of light, emit part of their energy as electromagnetic waves, if they are additionally accelerated by e.g. the Lorenz power of magnets. This emitted radiation is called synchrotron radiation and comprises a large range of wavelengths from the infrared to X-ray wavelengths. The radiation is distributed around a critical value λ_c which is given by:

$$\lambda_c = (4\pi r) / (3\,\gamma^3) \qquad (7)$$

with $\gamma = E/mc^2$, r = radius of the synchrotron ring in meters and E = energy of the particles. It is possible to separate a well-defined wavelength out of the continuous spectra of the synchrotron radiation using crystal monochromators (for monochromators see chapter 3.1). The intensity of the synchrotron radiation is mainly determined by the critical wavelength, the horizontal and vertical focusing of the beam and the reflection qualities of the optical elements within the beampath (mirrors and monochromators). The intensity can be augmented using additional magnets which further accelerate the moving particles (wigglers and undulators).

Synchrotron light is only emitted in the direction of movement of the particle and consequently the collimation of the beam is of extremely high degree (e.g. in comparison with X-rays) leading to a better resolution in the diffraction experiment compared to a conventional tube when proper optical elements are employed.

Furthermore due to the fact that the particles within the ring move in bunches, synchrotron radiation is therefore emitted in short pulses ($10^{-10}s$). This provides the means to observe very fast processes.

The third type of radiation used in modern crystallography is neutron radiation. Diffraction experiments using neutrons started in 1945 when the first reactor was developed. Neutrons are produced in a nuclear reactor by fission of heavy atoms like e.g. 235/92 U. The neutrons released in this reaction have kinetic energies of about 5*Mev* which corresponds to a wavelength of approximately 1.26×10^{-4}Å. To obtain neutrons suitable for diffraction experiments they have to be slowed down which is achieved by elastic collision with the nuclei of a so-called moderator. If the moderator is sufficiently thick the neutrons emerging will have a Maxwellian energy distribution with an average kinetic energy of $3/2\ KT$ (with K=Boltzmann‘s constant and T = temperature of the moderator). For a moderator at room temperature the kinetic energy of the neutrons is 0.04*eV* which corresponds to a wavelength of approximately 1.5Å.

Within a neutron reactor the flux of neutrons is relatively high. Yet the neutrons move in all possible directions and only very few of them (1 out of 10^5) travel in the direction of the collimator which leads to the diffraction experiment. Furthermore, only some of the neutrons which enter into the collimator have the correct wavelength to be diffracted by the monochromator crystal. All this leads to a comparatively low flux of neutrons at the sample (10^6 to 10^7 /cm^2/sec) compared to X-rays (10^{10} photons/cm^2/sec). Due to the lower cross section for neutrons than for X-rays (or electrons), the samples for neutron diffraction experiments have to be considerably larger than in X-ray diffraction and measuring times are usually longer.

The wavelength range for neutrons (taking into account hot and cold neutrons) lies between 0.5 to 10Å. The collimators in neutron diffraction are more complicated than in X-ray diffraction as the distance from the reactor to the samples is greater and cooling of the collimator is required.

Neutrons have a velocity distribution which follows the Maxwellian laws and there is a direct relationship between the wavelength of neutrons and the velocity which with they move. The choice of the employed wavelength is often realized using monochromator crystals (comparable to X-ray crystallography). Yet due to the relationship between wavelength and velocity of the neutrons it is also possible to use mechanical monochromators. The flight time for neutrons between the reactor and the sample lies in the range of 10^{-5} to 10^{-3}sec and therefore is is possible to use mechanical choppers to select the appropriate wavelength.

Important applications following from the relationship between velocity and wavelength of the neutrons are the so-called time of flight experiments. These experiments are based on the fact that if a pulse of neutrons of varying wavelength hits a sample, scattering will occur for all the wavelengths for which the Bragg equation is fulfilled. The scattered neutrons are counted by a neutron detector which is connected to a multichannel time analyzer. From an analysis of the distance from the specimen to the detector and the time needed the wavelength of the scattered neutrons is determined.

3.1 Filters and Monochromators

A beam of X-rays of a continuous wavelength range is called white radiation. While for some methods this white radiation is useful (Laue method), in the general application of X-rays for diffracting purposes a better monochromatized beam - comprising only a narrow range of wavelengths - is desirable. For monochromatization, two general methods are used. As mentioned above, the emission spectra of X-rays is specific for different chemical elements. The same holds for the process of absorption of X-rays (see Chapter 7.3.3). Every element has a specific absorption curve whose shape can be described by a series of single curves which do not meet continuously. The points of discontinuity are known as absorption edges and their position with respect to the wavelength is characteristic for an individual element.

While the absorption for a certain wavelength is high on the lower side of the absorption edge (i.e. at smaller wavelengths), the absorption drastically decreases just beyond the absorption edge. This effect is utilized in the β - filters (figure 8). For every target material there exists a chemical element whose absorption edge falls just between the K_α and K_β wavelength of the target material. Figure 8 illustrates the effect of a Zr-filter for Mo-target material.

While the K_β wavelength is absorbed to a high degree by the Zr filter, leading to a considerable drop of intensity for this wavelength, most of the intensity corresponding to K_α-radiation passes through. The result is an X-ray beam which is more monochromatic and now mainly determined by the K_α wavelength eliminating most of the unwanted K_β . Unfortunately, a loss in the intensity of the primary beam is unavoidable.

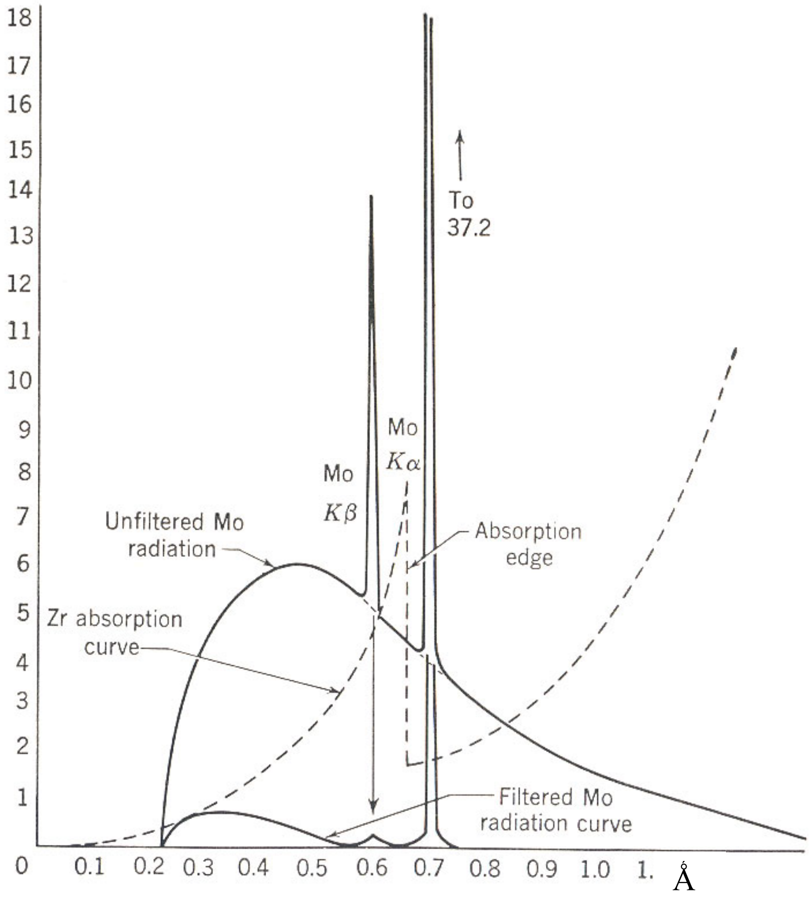

Figure 8: The action of filters in producing monochromatic X-rays.

An alternative way to produce monochromatic radiation is the use of a single crystal monochromator. According to Bragg's equation (Equation. 5) if a white beam hits a crystal the diffracted beams are observed at different Bragg angles Θ depending on the wavelength λ of the incoming beam. Thus the selection of a diffraction angle is equal to the choice of a the corresponding wavelength. The simplest monochromator is a single crystal cut with one face parallel to a major set of crystal planes.

A monochromator crystal has to be mechanically strong and stable under the influence of X-rays and the interplanar distance d within the crystal should be appropriate to select the desired wavelength. To reduce loss of intensity, the presence of strong diffracted intensities is indispensable. The mosaicity of the monochromator crystal determines the divergence of the primary beam and therefore the resolution at the sample.

On the other hand, the intensity *I* of the primary beam - especially in the case of synchrotron or neutron radiation -is mainly given by the width of the wavelength band which is cut out by the monochromator crystal(s) ($I \approx \Delta\Theta_m$).

3.2 Detectors

The first diffraction pattern was recorded in 1912 on a photographic plate. When an X-ray photon strikes the film it excites a silverhalide particle which, when the film is developed, produces a black silver grain on the film. The advantage of a photographic plate is that a lot of reflections can be recorded at the same time, yet the principal drawback (up to the invention of the densitometers) was the difficulty in relating the blackness of the film to the intensity of a reflection. With the invention of the Weissenberg camera in 1924 and the precession camera in 1942 recording and estimation of X-ray diffraction intensities on photographic film became the standard method for the determination of crystal structures for many years.

With the development of the automatic single crystal diffractometers the point detectors (scintillation and proportional counters) became the main devices to measure the intensities of X-rays. The main advantage of the point detectors is the higher precision in comparison to the film methods). The main drawback is that the reflections have to be measured one by one.

Modern area detectors (imaging plate and the CCD detectors) combine the high precision of the point detectors with the possibility to record more than one reflection at a time and thus considerably shorten the measuring times.

An imaging plate is essentially a storage phosphor. An X-ray photon produces on the plate a latent image that is excited by stimulation with a laser. This phenomena is called „photostimulated luminescence". The photostimulable material covering the plate is generally $BaFBr:Eu^{2+}$. When a photon hits the plate Eu^{2+} is oxidized to Eu^{3+}. The emitted electrons are trapped in Br vacancies (so called F centers) of the crystal. The electronic transition in these ions generates luminescence whose intensity is proportional to the intensity of the X-ray beam. The storage phosphor is read by an image reader which releases the information with the help of a laser and transmits it to a photomultiplyer tube. This tube converts the radiation to an electric signal. Afterwards the image plate is exposed to visible radiation which restores the initial conditions.

CCD detectors have a different way of operation (CCD stands for silicon chip charge-coupled device). Here X-ray photons are converted to visible photons by a phosphor. This signal is transferred to a CCD chip. The signal is stored in the pixels of the chip via the generation of electrons. The electrons are maintained by an imposed voltage till the readout when the charge stored is shifted to a readout amplifier. Every single row of pixels is then read out. A stationary controller converts the positions of the pixels with their charges to x, y coordinates on the detector face with corresponding intensities. These data are then written to a storage device.

4 Single crystal methods

4.1 The rotation method

One of the first film methods used in X-ray diffraction was the rotation method. To obtain a rotation photograph of a crystal, the crystal is mounted on a glass pin or in a capillary which is fixed to a goniometer head. The goniometer head allows for the necessary motions to center the crystal and to adjust one of its principal axes. In the first step one of the direct lattice axes has to be oriented normal to the incident beam direction. When this adjustment has been achieved a family of equidistant reciprocal lattice planes is parallel to the incident beam direction.

With a position of the crystal only very few points fulfill the diffraction condition and therefore to obtain more diffraction spots from other planes the sample is rotated with the rotation axis perpendicular to the primary beam.

Whenever a reciprocal lattice point passes through the Ewald sphere a diffracted beam passes in turn through this point. These points lie on equidistant circles of decreasing radii when one moves away from the center of the Ewald sphere. A cylindrical cassette with photographic film is placed around the crystal with the cylinder axis coinciding with the rotation axis. The circles then project undistorted unto the film and if the film is unrolled straight lines of diffraction spots appear. These diffraction spots are arranged in exactly horizontal layer lines provided the crystal is well adjusted. (Figure 9, 10).

The layer line that passes through the undeviated beam stop is the zero layer line; the others are numbered above and below accordingly. For a crystal rotated along *c** the Miller indices of these layer lines are *hk0*, *hk1*, *hk2* etc. and accordingly the value of *c** can be calculated from the line spacing of the corresponding rotation photograph.

The oscillation method is practically the same only that the crystal is not rotated by a full 180^0 but only $5\text{-}20^0$ degrees to avoid overlap of reflections and reduce exposure time.

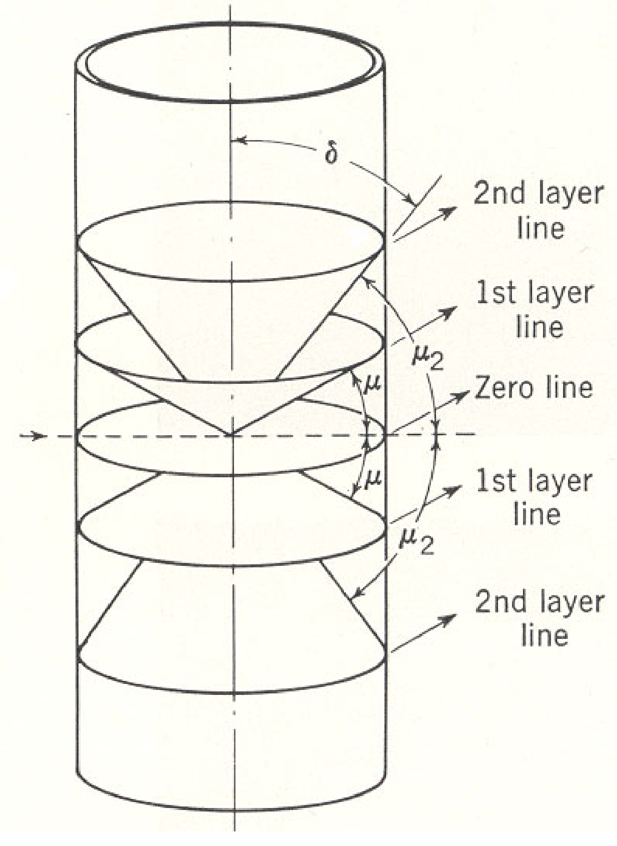

Figure 9: Schematic rotation diagram on a cylindrical film.

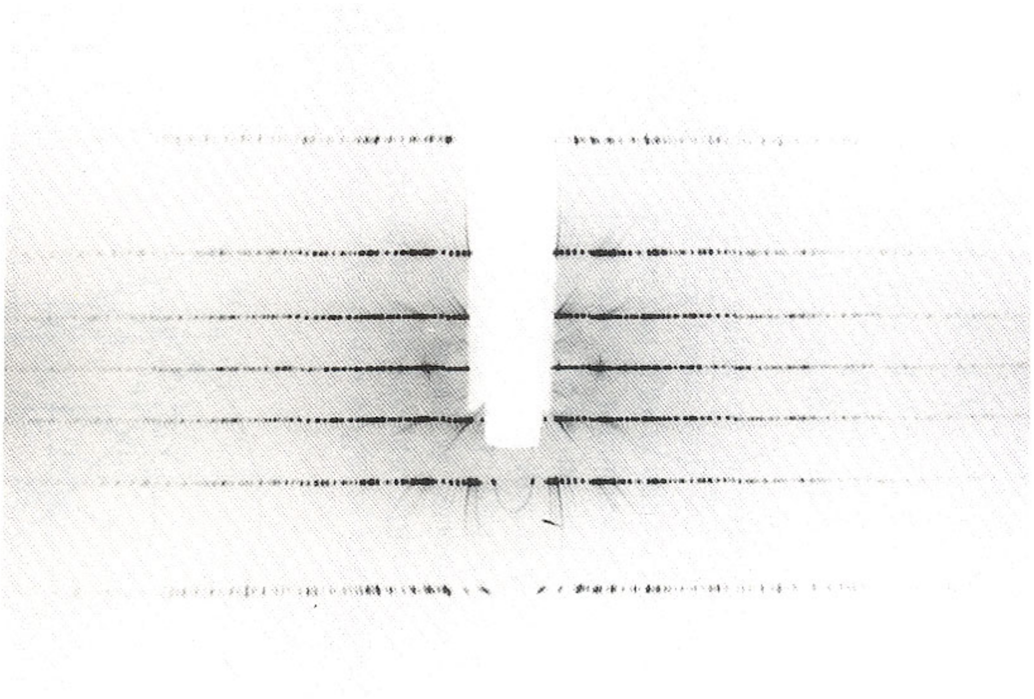

Fig .10: A typical rotation photograph.

4.2 The Weissenberg camera

In a rotation photograph one of the indices of reflections (corresponding to the layer direction) is trivial to assign. Yet the other two indices within the layer are complicated to determine as a whole layer is projected onto one line. To overcome this difficulty the Weissenberg method was invented in 1924. Two main differences with respect to the rotation method are as follows: Firstly, layer line screens are introduced which block all other layers but the one to be examined. Secondly, the rotation of the crystal is coupled to the translation of the photographic film systematically. As a consequence a Weissenberg photograph is a mapping of one single reciprocal lattice plane onto the film plane.

A schematic drawing of a Weissenberg camera is given in figure 11. Worm A moves the film from left to right while worm B rotates the crystal synchronously with this translation. Due to the translation of the film the spots from a chosen layer are distributed over the entire film and not projected onto a single line as in a rotation photograph. If Worms A and B are uncoupled a simple rotation photograph can be accomplished.

To produce a Weissenberg photograph the crystal is centered and a lattice plane is pre-adjusted optically. With the help of oscillation photographs one lattice plane is perfectly adjusted and the lattice parameter corresponding to the distance between different layers can then be extracted. Now one of the lattice planes is separated with the layer line shields. Normally the zero plane is first recorded. In the case of z as rotation axis the zero layer plane would correspond to the *hk0* plane.

In the Weissenberg film (see figures 12 and 13) two main reciprocal lattice axes are projected as straight lines. Furthermore festoon families can be observed. A single festoon corresponds to one reciprocal space line and therefore all reflections on it have one index in common. With the help of a special net the diffraction spots on the film can be easily indexed and the corresponding *d*-values can be calculated.

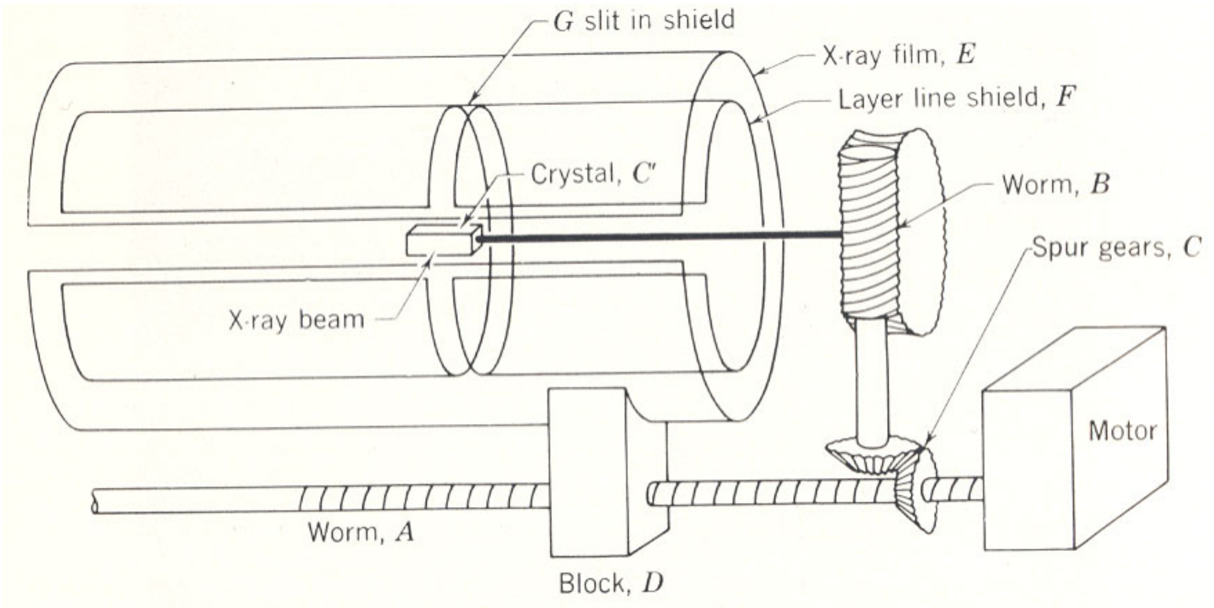

Figure 11: Schematic drawing of a Weissenberg camera.

A *hk0* layer Weissenberg photograph yields three lattice parameters: *a*, *b* and the corresponding angle between them (= γ). To record higher layers (*hk1, hk2…)* a Weissenberg camera has further adjustment possibilities. Thus the rotation axis of the crystal can be turned away from the normal-beam direction. This movement requires the translation of the layer line shields.

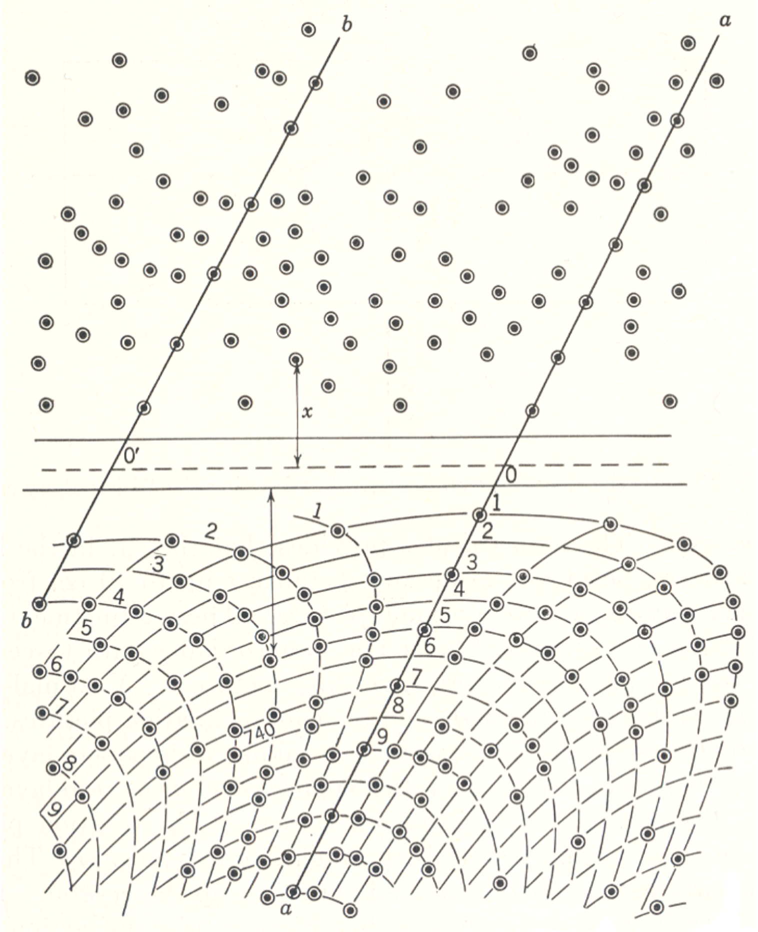

Figure12: A schematic representation of a Weissenberg photograph

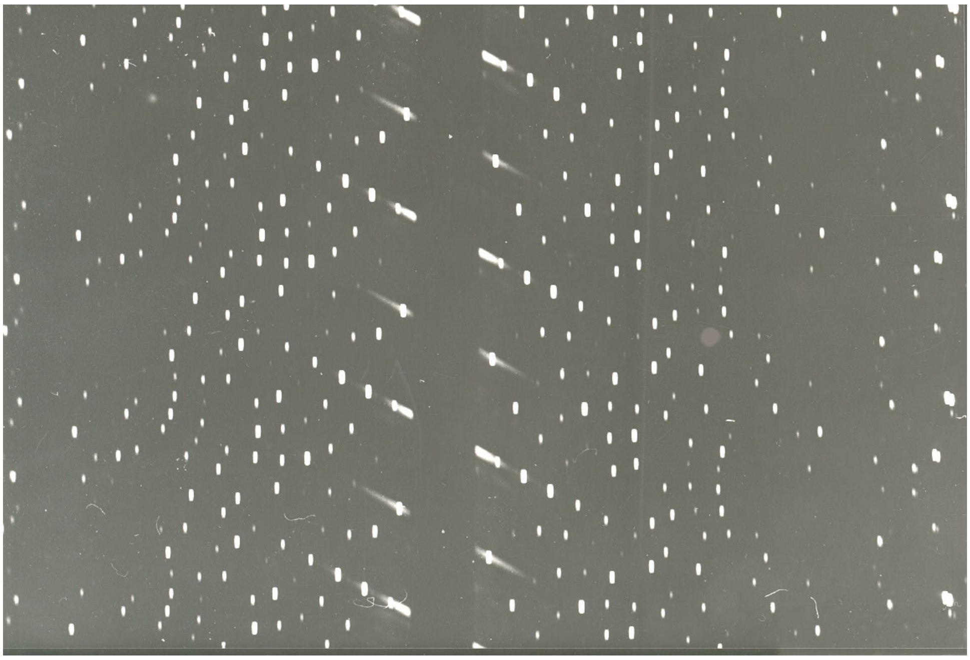

Figure 13: Zero level Weissenberg photograph of the mineral cancrinite.

4.3 The Precession camera

In the Weissenberg method the reciprocal lattice planes are projected in a distorted way. On the other hand, the precession method produces an undistorted picture of reciprocal lattice planes which can easily be interpreted. A disadvantage with respect to the Weissenberg method is the limited information about the higher Θ range and the existence of blind regions spots i.e. the impossibility to record certain parts of reciprocal space.

For the precession method one of the axes is adjusted parallel to the X-ray beam. Then a set of lattice planes is tangent to the Ewald sphere. The crystal is then rotated in such a way that the normal of this plane makes a precessing motion i.e. the normal always keeps a constant precession angle μ around the primary beam. The film is moved in an identical way and is thus always adjusted parallel to the reciprocal lattice plane (Figure 14).

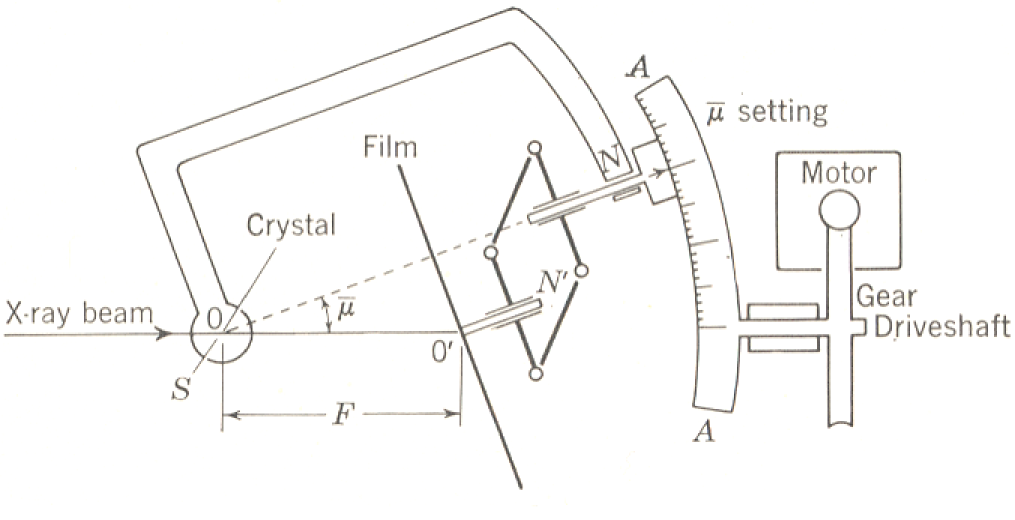

Figure 14: A schematic representation of a precession camera.

When a full revolution of the plane normal about the X-ray beam has been completed the intersection of the reciprocal lattice plane with the Ewald sphere describes a circle with the radius *r*

= 2 sin μ_p / λ and all points of the reciprocal lattice which are within this sphere have produced diffraction spots on the film. Every point crosses the Ewald sphere twice and they will only superimpose exactly if the reciprocal lattice plane is perfectly adjusted. If this is the case the precession photograph is an undistorted recording of a reciprocal lattice plane (see Fig 15). Accordingly from one photograph two lattice parameters as well as the angle between them can be determined.

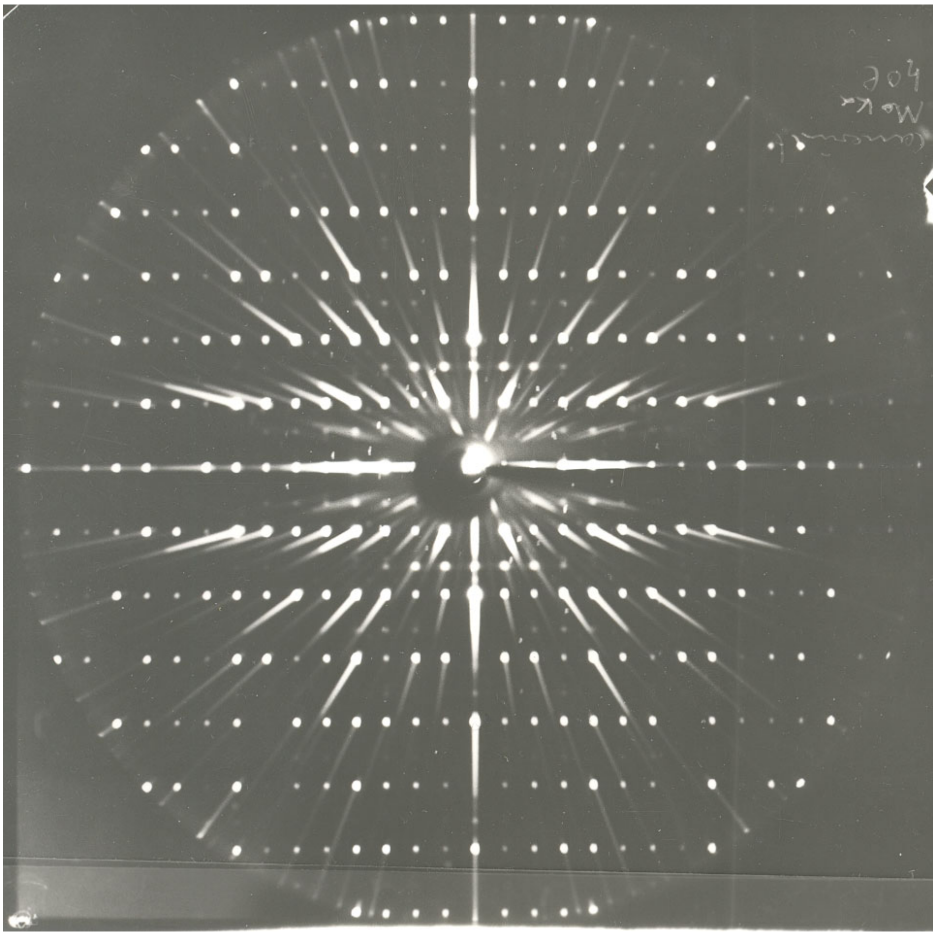

Fig 15: Zero level precession photograph of the mineral cancrinite.

To record only one layer at a time line screens must be used. To record higher layers the film center has to be moved and the distance between crystal and film cassette has to be adjusted. The corresponding μ_p is calculated and employed. It is an innate property of the method that in higher layers a blind spot occurs close to the primary beam spot on the film.

4.4 The automatic single crystal diffractometer

The main advantage of a single crystal diffractometer in comparison to film methods is the higher precision and the better estimation of the standard errors of the measured intensities. The main disadvantage is that point detectors can record only one reflection at a a time (this is mainly overcome by the use of CCD detectors and Imaging plates).

A single crystal diffractometer consists basically of four parts: the X-ray tube, the X-ray detector, the goniometer for orienting the crystal and the computer for registration and evaluation of the obtained data. The X-ray tube and the generation of X-rays as well as the main types of detectors have been described in chapter 3.

A four circle diffractometer has generally equatorial geometry i.e. the diffracted beams are measured in the horizontal plane which is defined by the primary beam and the rotation of the detector. The detector moves in this plane and forms an angle of 2Θ with the primary beam. A lattice point in diffraction position cuts the Ewald sphere and produces a secondary beam which can only be detected if it is in the equatorial plane of the detector. Therefore to observe the diffracted intensity the reciprocal lattice points have to be brought to the 2Θ circle. The detector is then moved to the appropriate position to receive the diffracted intensity.

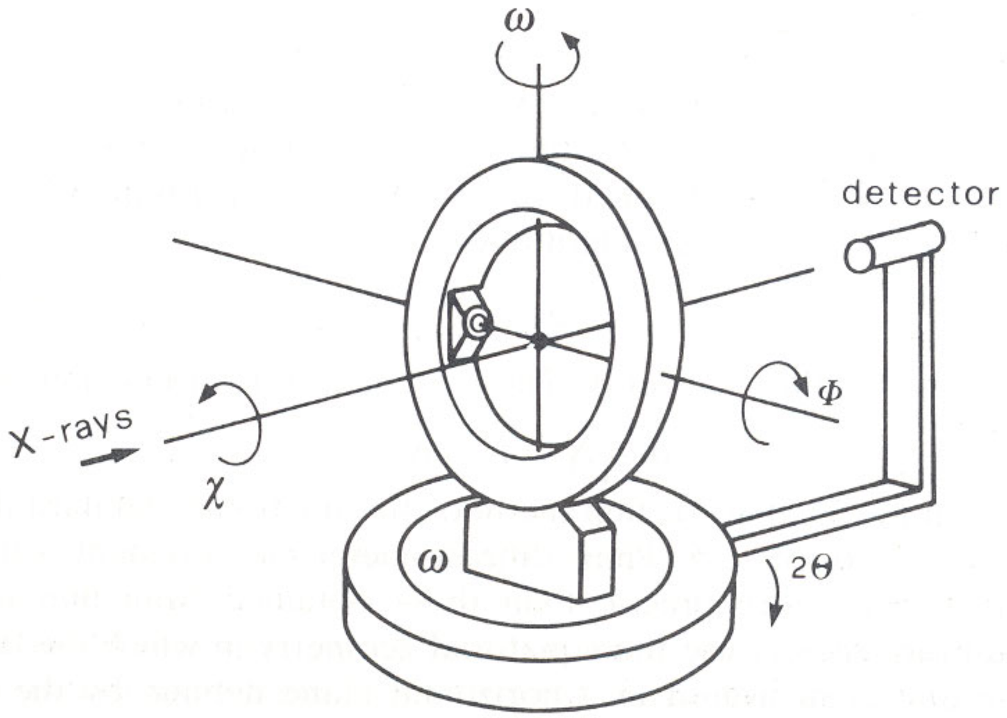

Figure 16: Schematic drawing of a single crystal diffractometer with Euler geometry.

Two main geometries are used for single crystal diffractometers: the Euler and the Kappa geometries. In the first (Figure 16) the χ circle carries the goniometer head with the crystal. The main axis of the goniometer is normal to the equatorial plane and to the incident and diffracted beam. The rotation of the cradle around this axis defines the angle ω. The rotation around the spindle axis of the goniometer head defines φ and is basically equivalent to the rotation axis in film methods. χ is the angle between the spindle of the goniometer head and the main instrument axis. Thus χ and φ describe the rotations of the crystal, while ω characterizes the rotation of the cradle. Finally 2Θ is the angle that defines the rotation of the detector.

The two rotations φ and ω are necessary to bring a reflection onto the Ewald sphere and the rotation around χ is then used to move the reflection into the equatorial plane (Figure 17). At last the detector is moved into the appropriate 2Θ position to record the diffracted intensity.

The alternative to the Euler geometry is the Kappa geometry. Here the χ circle does not exist and is substituted by the κ arm. This arm can rotate about the κ axis which forms an angle of approximately 50^0 with the main instrument axis. The advantage of this geometry is that more space is available to mount e.g. cooling or heating devices. Since more rotations are possible and less collisions do occur, more data points can be measured.

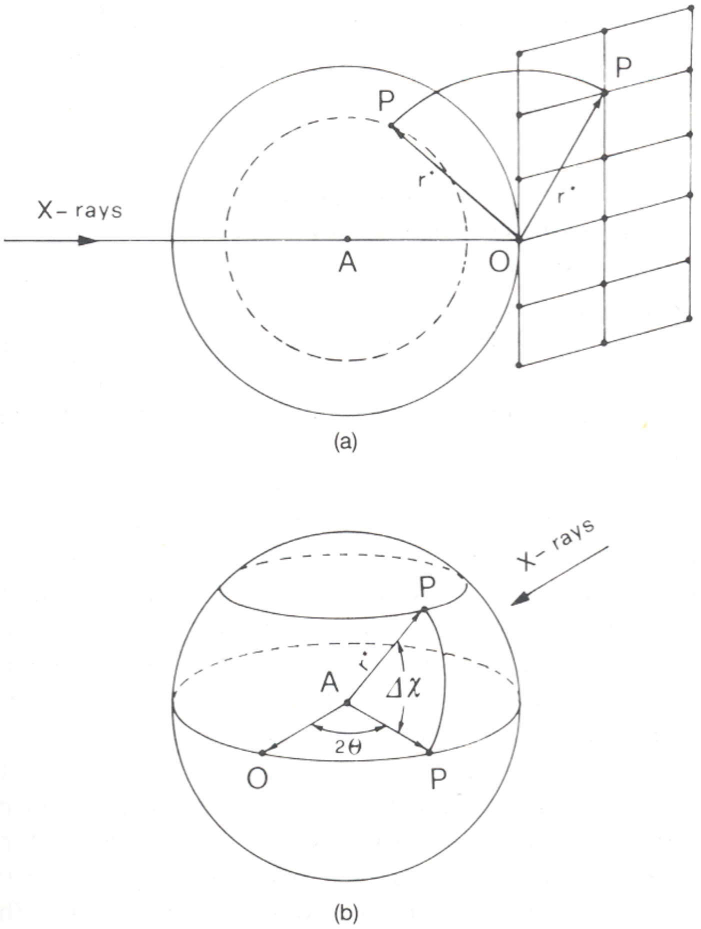

(a)

(b)

Figure 17: Necessary steps to bring a lattice node to the intersection of the Ewald sphere and the equatorial plane of the diffractometer.

A diffractometer measurement normally follows the same basic scheme which will be briefly outlined here. The crystal is mounted on a goniometer head and the orientation matrix is determined. This matrix describes the position of the main crystallographic directions with respect to the diffractometer axes. Once the orientation matrix is known it is possible to calculate the angles and to bring any *hkl* into diffraction position. It is important that the entire volume of the lattice node passes through the Ewald sphere.

To obtain the integrated intensity from the measured profile the linearly estimated background of the peak is simply subtracted form the total counts. Far more sophisticated profile analysis is also applied in some cases. The so calculated integrated intensities have to be corrected for several physical correction factors (see chapter 7.3).

The main disadvantage is that not the whole reciprocal space is recorded but just some well defined positions which are calculated via the orientation matrix. Thus if this method is not combined with e.g. film methods diffuse scattering or weak reflections can easily be overseen. With the introduction of area detectors in automatic single crystal diffractometers this disadvantage is mainly overcome.

5 Powder diffraction

5.1 The characteristics of a powder diffraction pattern

A powder can be regarded as a polycrystalline mass (figure 18) with crystallites in all possible orientations. 1cm^3 of powder contains approximately 10^9 particles for 10µm crystallites and 10^{12} particles for 1µm crystallites.

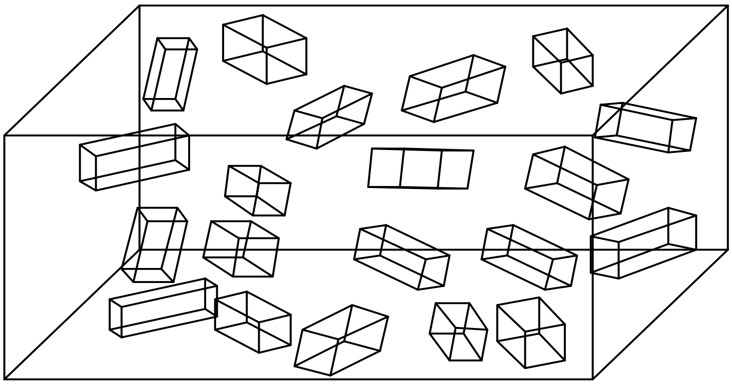

Figure 18: Schematic view of different orientations of the crystallites in a powder.

Due to the large number of orientations of the crystallites in a powder, the single crystal reciprocal lattice is smeared into spherical shells (figure 19). In other words, the three dimensional reciprocal space **Q** is projected onto the one dimensional 2Θ (= $|Q|$) axis. In real space (crystal space), the information of reflections having the same d-spacing is distributed over so called Debye-Scherrer cones (figure 19)

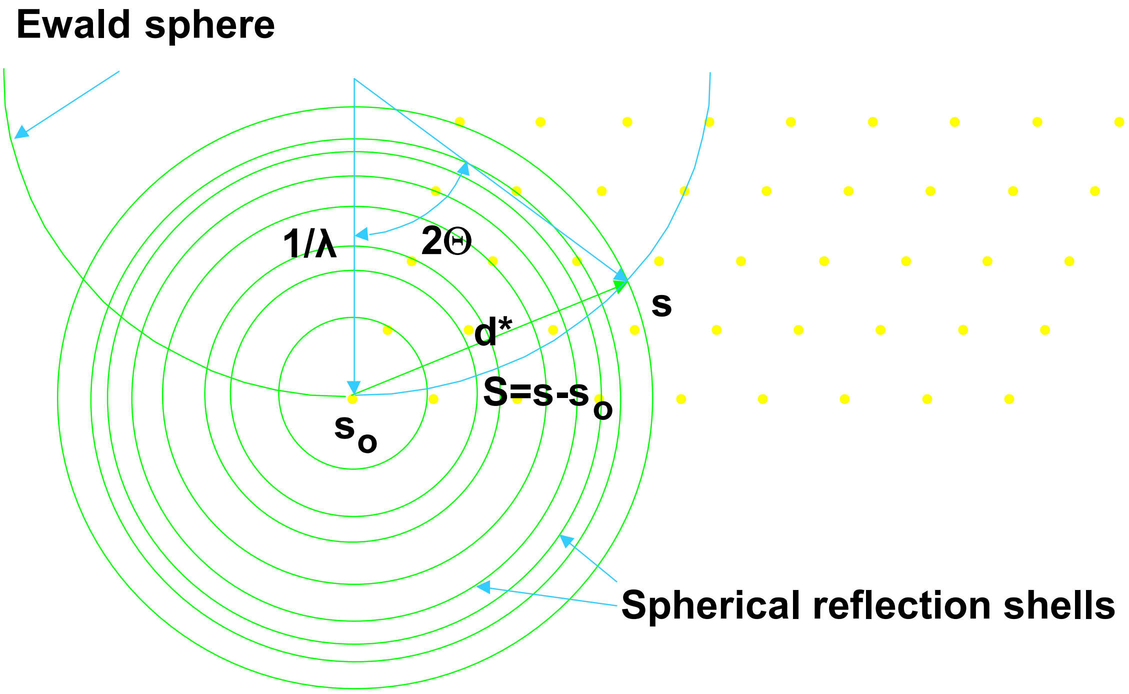

Figure 19: Powder diffraction in reciprocal space

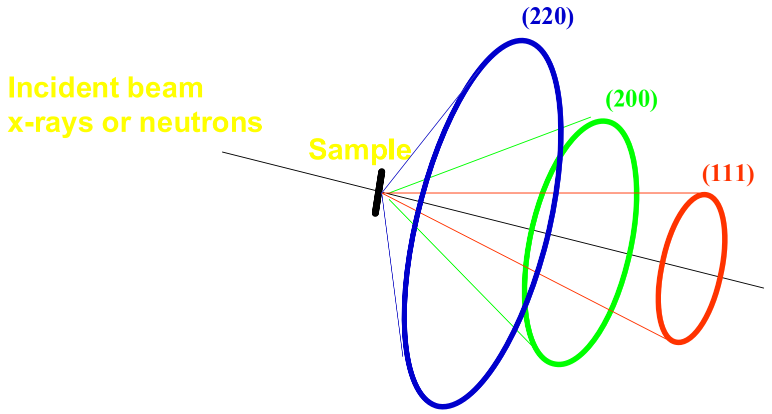

Figure 20: Debye-Scherrer cones in real space. Suitable 2-dimensional detectors are film or image plates. 1-dimensional detectors are i.e. scintillation detectors or 3He tubes (neutrons).

Despite the early development of the powder diffraction method in the year 1916, just 4 years after the first single crystal diffraction experiment, the method was used for almost half a century almost exclusively for qualitative and semi-quantitative phase analysis. This changed completely with the development of the Rietveld method, a technique for the refinement of crystal structures using the entire information of a powder diffraction pattern, in the year 1969. Starting in the middle of the seventies, *ab-initio* crystal structure determinations from powder diffraction data using basically methods adapted from single crystal structure determination are found occasionally in the literature. Nowadays, a variety of new algorithms for structure determination from powder diffraction data have been developed and crystal structure determination of complex framework structures (e.g. zeoliths) or even molecular crystal structures of pharmaceuticals is becoming a routine procedure. The recent success of the powder method is due to three advances: the optimization of the measurement, the accurate description of the profile of a powder diffraction peak and the data reduction algorithms. It is noteworthy that the general availability of synchrotron radiation advanced the powder method considerably. Because of the parallel, highly monochromatic very intensive synchrotron X-ray beam, neighboring Bragg reflection can be well separated and their individual intensities can be determined with high precision. The logical result is higher accuracy in the determination of atomic positions and bond lengths, allowing a better interpretation of the mechanisms of bonding and reactions. Another advantage, which is particularly valuable for mineralogical work is the qualitative and quantitative analysis of extremely small amounts of material. Last but not least, the possibility to quickly change the wavelength over a large energy range enables the use of anomalous dispersion to distinguish between elements with almost equal scattering power and so called “depth profiling” of thin coatings due to the energy dependence of the penetration depth. The latter is useful e.g. in apatite coated artificial limbs.

A physically meaningful description of the powder reflection profile in combination with high resolution data allows the extraction of details of the microstructure like lattice strain, domain size and disorder (e.g. stacking faults in clay minerals). As a side effect of the better description of the powder peak profile, structural details like the positions of extremely weak scattering hydrogen atoms (as in the case of high pressure minerals with hydroxy-groups) become visible.

Two competitive type of algorithms for structure determination from powder diffraction data are available which operate either in *direct* or in *reciprocal* space. The conventional methods like Patterson- and Direct Methods rely on the number of precisely determined integral intensities of individual Bragg reflections, which restricts their use in powder diffraction to crystal structures with a maximum of 20-30 atoms in the asymmetric unit. Recently, so called **direct space methods** (not to be confused with direct methods) like the simulated annealing technique have been developed which are capable of solving more complex structures in a short period of time. The only drawback of direct space algorithms is that the connectivity of atoms must be known *a priori*, which is not always the case for mineralogical problems.

Recently, the substitution of X-ray sensitive photographic films by image-plates with short exposure times and a huge linear dynamic range allows structure refinements and -determinations as a function of pressure, temperature and during chemical reactions *in situ*, which opens new perspectives for experimental mineralogy.

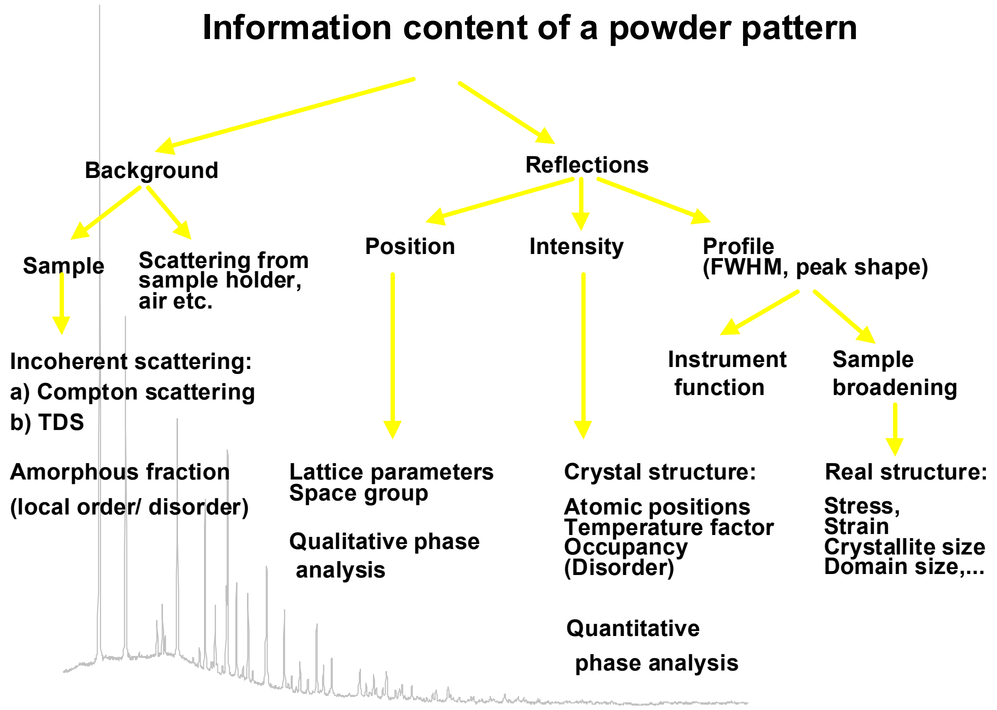

Figure 21: Content of information of a powder diffraction pattern.

Figure 21 illustrates the amount of information which can be extracted from a powder diffraction pattern. The goal for a systematic evaluation of a powder pattern is to extract as much information as possible in a routine manner.

5.2 Measurement of a Powder Pattern

The resolution of a powder diffraction pattern is defined by the full width at half maximum of the individual Bragg reflections (FWHM). The breadth of a peak is a function of the optics of the diffractometer (instrumental broadening) and the sample (sample broadening).

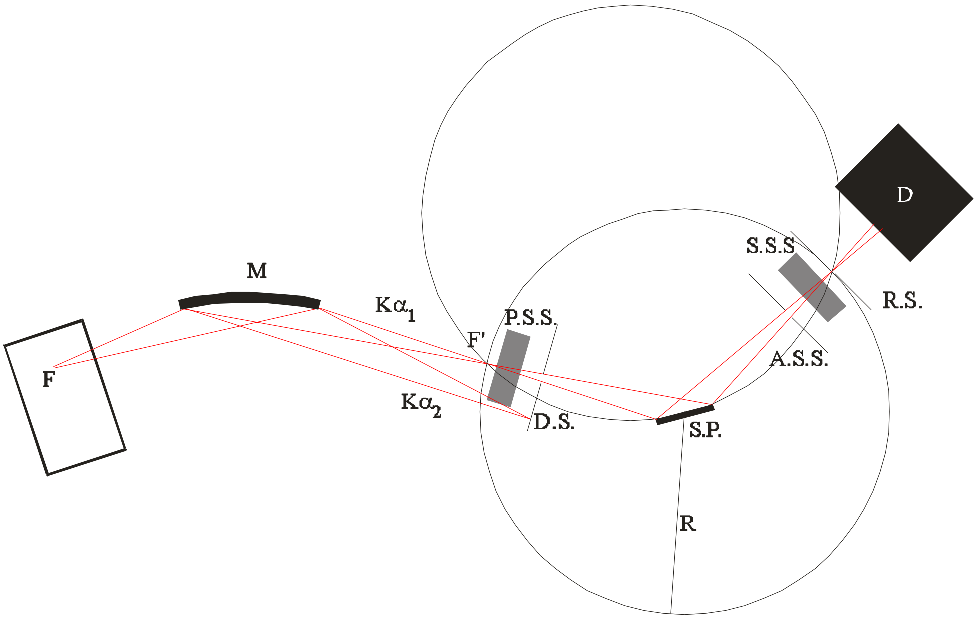

Figure22: Modern Bragg-Brentano laboratory diffractometer in reflection geometry with bent (focusing) primary beam monochromator M, primary soller slit P.S.S., divergence slit D.S., scattering slit A.S.S., secondary soller slit S.S.S and receiving slit R.S.

One possibility to improve the resolution of a powder diffraction pattern in order to gain more information for the determination of crystal structures is the minimization of the instrumental broadening. The basic requirements for good instrumental resolution are monochromatization and collimation of the X-ray beam which can be achieved using primary- and secondary beam monochromators simultaneously. The lower limit of the resolution is then given by the intrinsic Darwin widths. In a typical laboratory instrument with divergent beam from a X-ray tube, typically a bent focusing single crystal primary beam monochromator after Johansson is used (figure 22).

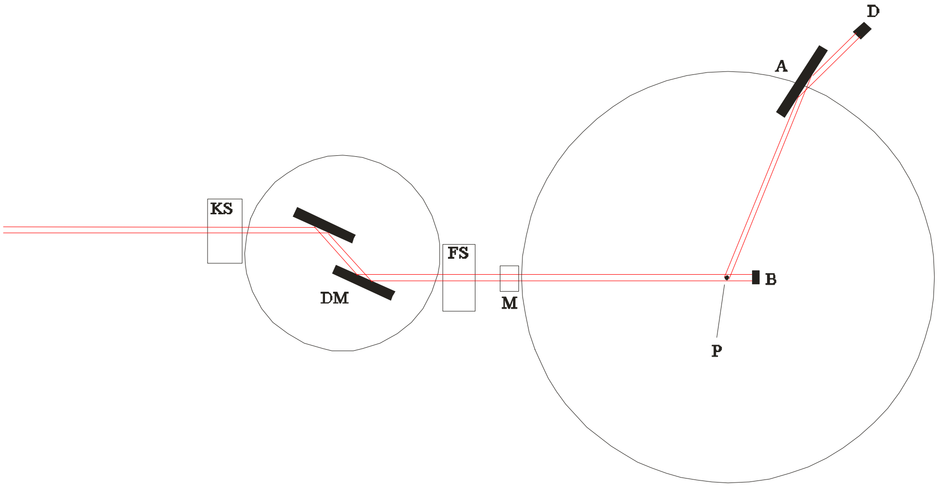

Figure 23: Parallel beam geometry in Debye-Scherrer mode using a double monochromator (DM) and an analyzer crystal (A) at a synchrotron as realized e.g. at BM16 (ESRF) or X3B1 (NSLS)

Secondary beam monochromators for laboratory instruments are mainly used to reduce fluorescent scattering. A combination of both types of monochromators would result in an unacceptable decrease of scattered intensity and is usually not used in the home laboratory. For the comparatively divergent X-ray beam, the achievable resolution is mainly determined by the opening of the receiving slit (R.S. in figure. 22) in front of the detector. The minimum FWHM of the geometry as shown in figure 22 using Cu-Kα_1 radiation is close to 0.035°2Θ. At a high resolution powder beamline at a synchrotron with parallel beam geometry, the resolution is not determined by slits but by the *d*-spacing of the analyzer crystal (secondary beam monochromator) which is typically an order of magnitude better, $\frac{\delta d}{d} \approx 1 \cdot 10^{-4}$ (figure 23). It should be noted that the FWHM strongly depends on the energy (wavelength) of the X-rays, although the resolution is nearly the same.

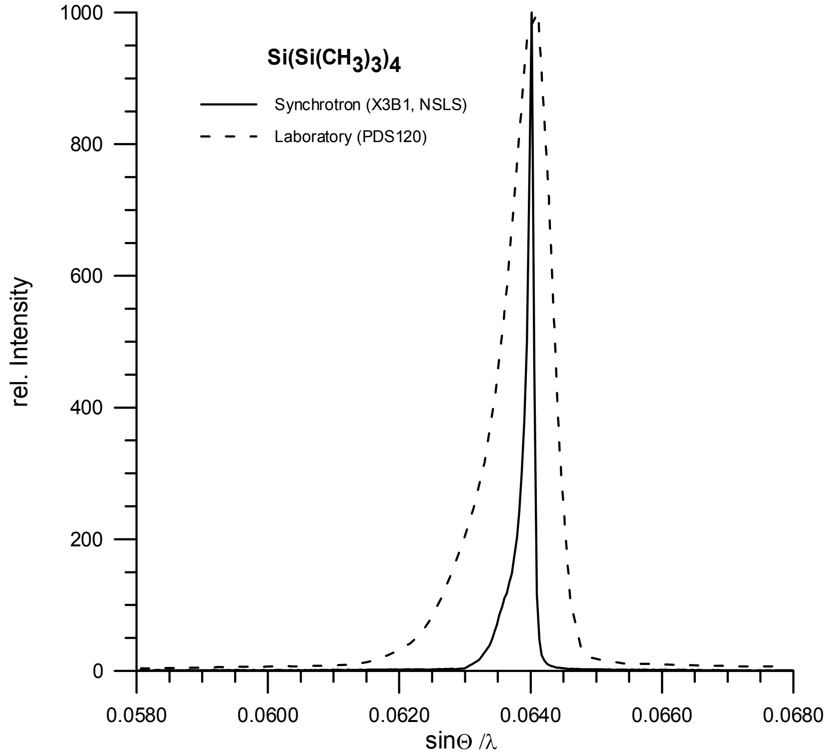

Figure 24: Direct comparison of the FWHM of tetrakistrimethylsilylsilan in transmission geometry at room temperature, measured at a Synchrotron (X3B1, NSLS) (solid line) and in the laboratory (PDS120 of Nonius BV) (dashed line).

A direct comparison of the instrumental resolution between a typical laboratory diffractometer with primary beam monochromator in transmission geometry and a high resolution synchrotron instrument is possible when FWHM is expressed in a wavelength independent term like sinΘ/λ, pretending that the standard sample has virtually no sample broadening effects.

Besides the high intensity and brilliance as well as the high angular and energy resolution of the synchrotron radiation, the better reflection to background ratio, the negligible instrumental contribution to the FWHM and the possibility to perform transmission measurements at very high energy (low wavelength) are important arguments to prefer the synchrotron source to conventional X-rays (figure 24).

In general, reflection geometry (Bragg-Brentano) is the method of choice for strongly absorbing sample with the disadvantage of being sensitive to grain size and preferred orientation effects (figure 25). These effects are reduced in transmission mode (Debye-Scherrer) mode which on the other hand is sensitive to the effect originating from the absorption of the sample. Until recently, the only way to reduce the absorption for samples containing strong scatterers was the dilution of the material with amorphous material like powderized cork in combination with thin capillaries. With the availability of high energy synchrotron beamlines like ID15 (ESRF) virtually any sample can be measured in transmission geometry without the need for absorption corrections.

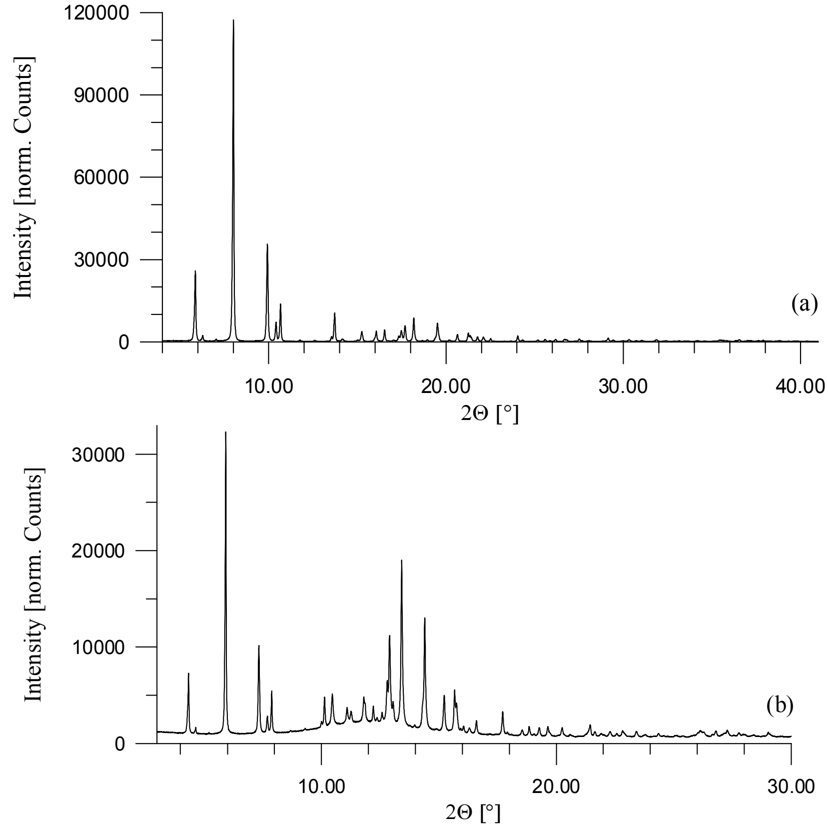

Figure 25: Powder diffraction patterns of the same pigment measured in reflection geometry at beamline X3B1 (NSLS) (top) and in transmission geometry at beamline BM16 (ESRF) (bottom) (Note the difference in the angular scale due to different X-ray wavelengths).

Another advantage of synchrotron radiation is the possibility to quickly tune the wavelength within a wide energy range which allows the use of the anomalous dispersion effect (see chapter 7.1) to distinguish between heavier elements with almost identical number of electrons or to perform so called 'depth profiling' by making use of the energy dependency of the penetration depth of the radiation (see chapter 11.3).

Furthermore, synchrotron radiation is almost 100% polarized and parallel beam geometry produces simple line shapes (see chapter 8.1) suitable for the analysis of the microstructure.

It should be noted that the real width of a Bragg reflection is mainly determined by the sample induced broadening due to grain (domain) size (see chapter 8.3.1) and by microstrain (see chapter 8.3.2). Therefore, there is no advantage in measuring poorly crystalline powder at a synchrotron.

6 The position of a Bragg reflection

The dimensions of the unit cell exactly defines the positions of the Bragg-reflections. If the unit cell parameters are known, indexing of the diffraction pattern can be done by applying the general formula:

$$\begin{aligned}
Q_{hkl} &= d^{*2} \\
&= \frac{1}{d^2} \\
&= \frac{4\sin^2\Theta}{\lambda^2} \\
&= h^2 a^{*2} + k^2 b^{*2} + l^2 c^{*2} + \\
&\quad 2hka^* b^* \cos\gamma^* + 2hla^* c^* \cos\beta^* + 2klb^* c^* \cos\alpha^* \\
&= h^2 A + k^2 B + l^2 C + hkD + hlE + klF
\end{aligned} \tag{8}$$

with

$$a^* = \frac{bc\sin\alpha}{V},$$

$$b^* = \frac{ac\sin\beta}{V},$$

$$c^* = \frac{ab\sin\gamma}{V},$$

$$\cos\alpha^* = \frac{\cos\beta\cos\gamma - \cos\alpha}{\sin\beta\sin\gamma},$$

$$\cos\beta^* = \frac{\cos\beta\cos\gamma - \cos\alpha}{\sin\beta\sin\gamma},$$

$$\cos\alpha^* = \frac{\cos\beta\cos\gamma - \cos\alpha}{\sin\beta\sin\gamma},$$

$$V = abc\sqrt{1 + 2\cos\alpha\cos\beta\cos\gamma - \cos^2\alpha - \cos^2\beta - \cos^2\gamma}$$

where a, b, c, α, β, γ, and V are the lattice parameters and the volume of the unit cell, whereas the superscript * denotes their values in reciprocal space. Indexing of a single crystal diffraction pattern is usually trivial if one employs methods like Weissenberg or precession (see chapter 4.2, 4.3). On the single crystal diffractometer the indexing is equivalent to determining the orientation matrix of the crystal (see chapter 4.4). Problems which are encountered when using indexing routines for a single crystal pattern are normally due to twinning i. e. the existence of several single crystalline individuals in different orientations.

The indexing of a powder pattern without knowing the lattice parameters is a non-trivial task. There is no guarantee that a powder pattern can be indexed and it is commonly necessary to try out different computer programs employing different algorithms. The method of choice strongly depends on the symmetry of the crystal system. The difficulty lies in the proper selection of reflections for the determination of the reciprocal lattice parameters. A large number of combinations must usually be tested before the correct lattice can be found.

After indexing of a sufficient number of reflections the lattice parameters can be refined using the method of least squares. Once a set of lattice parameters has been obtained, it is strongly recommended to check them against all measured reflection positions e.g. by applying a Pawley- (chapter 10.2.3) or LeBail-fit (chapter 10.2.2).

The positions of Bragg reflections in a powder diffraction pattern are often affected by systematic aberrations arising either from the sample itself or from an improper setting of the sample or diffractometer. These shifts relate to errors having a constant, a cosΘ and a sinΘ dependency, respectively. The corresponding errors originate from different physical or/and geometrical problems depending on the diffraction geometry. Here, the sample displacement error is one of the largest systematic errors affecting line positions and is based on the fact that the sample surface is displaced with respect to the axis of the goniometer.

7 The intensity of a Bragg reflection

7.1 The atomic form factor

Atoms are not point-like objects in a mathematical sense. Their 'radius' is of the order of X-ray wavelengths and as the electrons are distributed over the entire atomic volume, there will be phase differences which decrease the intensity of the scattered wave with increasing scattering angle Θ (figure 26). This decrease is described by the atomic form factor f_0.

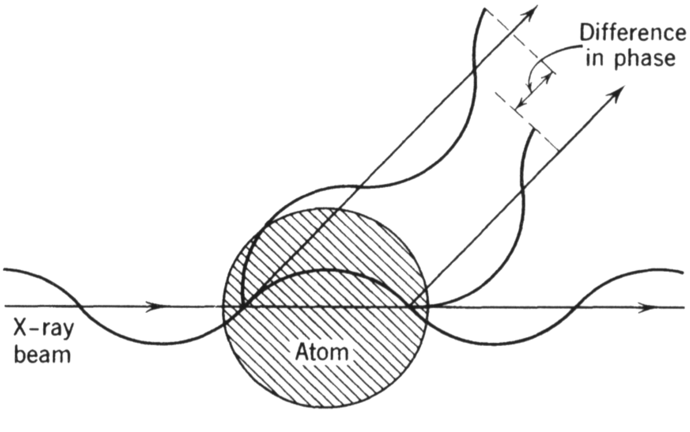

Figure 26 Phase difference of X-rays which are scattered at different locations within an atom.

The numerical values for the atomic form factors (figure 27) for most atoms and ions are tabulated in volume III of the International Tables for Crystallography.
In contrast to X-rays, neutrons interact with the atomic core, making them sensitive for light elements like hydrogen and oxygen. The 'visibility' of elements for neutrons does not depend on the number of electrons like in the case of X-rays (figure 28) and elements which are neighbors in the periodic system may have entirely different neutron scattering cross sections.
The tabulated form factors (figure 27) are only valid at T= 0K. Therefore a correction term T_{hkl}, the so called Debye-Waller or atomic displacement factor was introduced. This factor describes the thermal motion of the atoms which destroys the ideal phase relation between the atoms of the lattice planes and decreases the scattering amplitude (figure 29).

$$f\left(\frac{\sin\Theta}{\lambda}\right) = f_0\left(\frac{\sin\Theta}{\lambda}\right)T_{hkl},\ T_{hkl} = \exp\left(-B\frac{\sin^2\Theta}{\lambda^2}\right) \tag{9}$$

with

$$B = 8\pi^2\overline{u}^2\left[\text{Å}^2\right]$$

where $\overline{u}$ describes the average elongation of the atom perpendicular to the reflecting lattice plane.

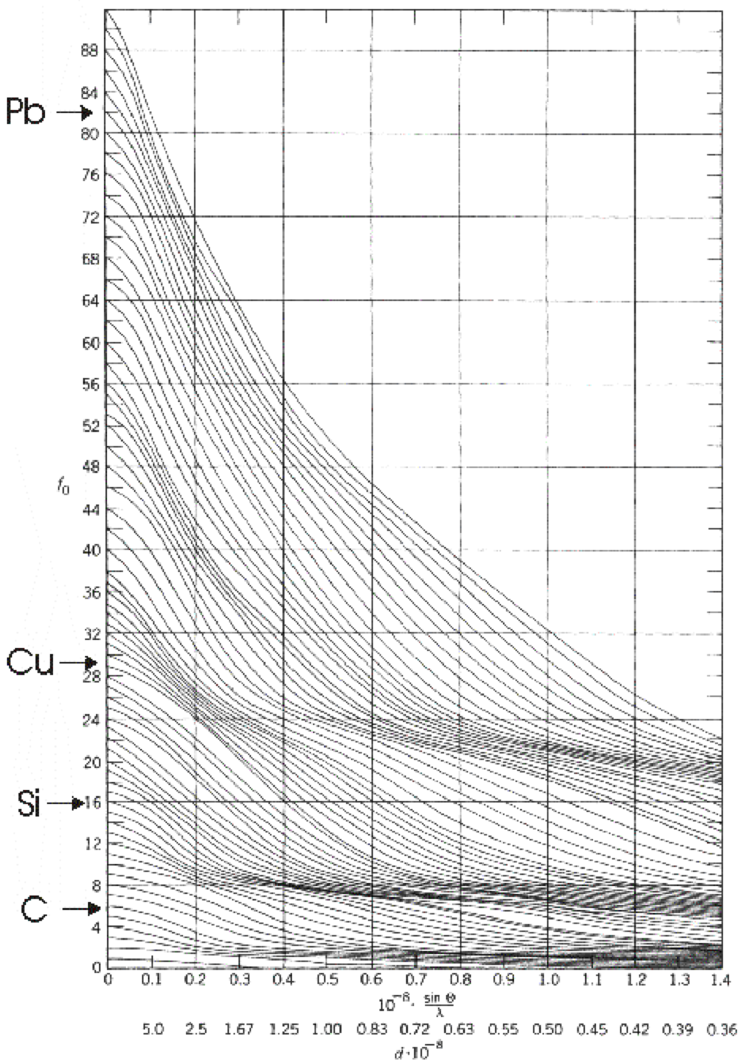

Fig 27: Atomic form factors as a function of sinΘ/λ for atoms (charge 0). The numbers of the y-axis correspond to the atomic number Z of the elements.

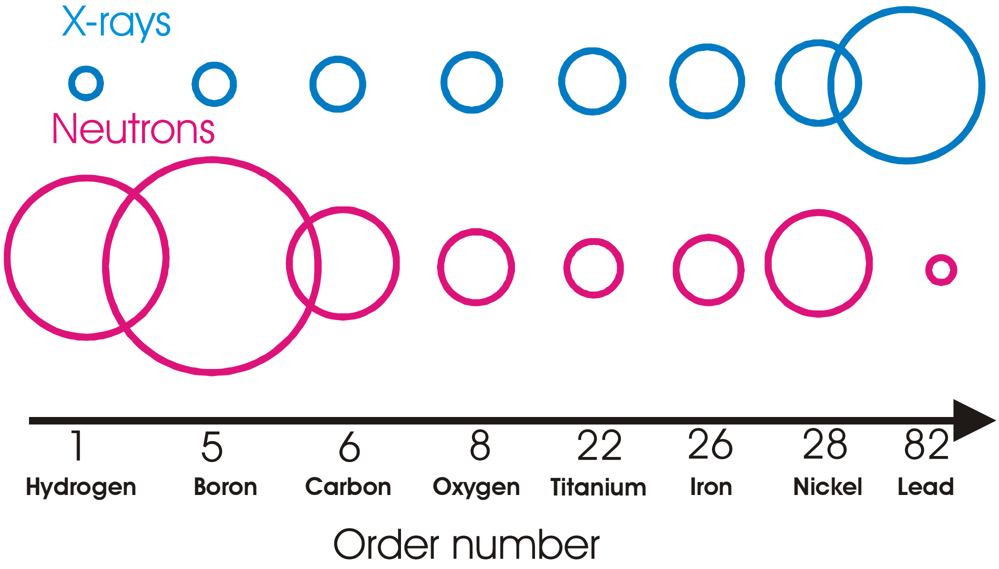

Figure 28: 'Visibility' of selected elements for X-rays (top) and neutrons (bottom).

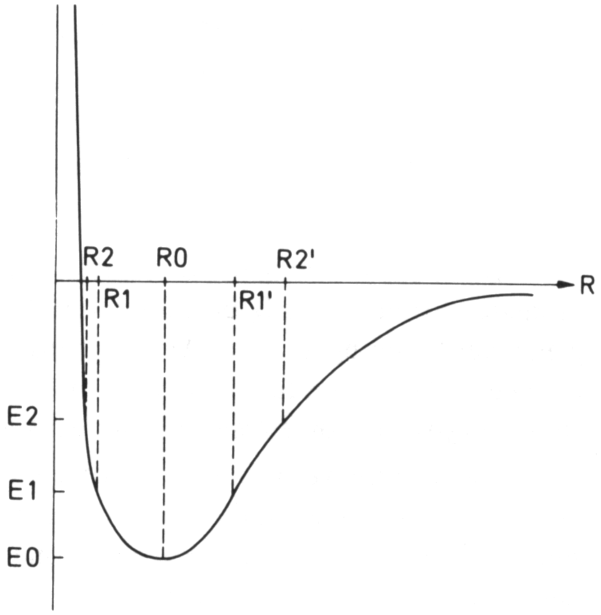

Figure 29: With increasing temperature (energy E), atoms swing between two energetic equivalent positions R and R', creating additional phase differences which decrease the intensity of the scattered radiation.

The average thermal motion of an atom does not have to be equal in all directions and therefore anisotropic displacement parameters are used to achieve a better description. Generally, the anisotropic displacement factor is expressed by a tensor of second order, yet more anharmonic conditions can be described using tensors of higher order.

A good estimation of the anisotropic displacement parameters requires an excellent parameter to observation ratio. This is normally not the case in powder refinement and therefore only isotropic displacement parameters are refined here (often it is even enough to refine an overall temperature factor common to all atoms).

In single crystal refinements the anisotropic displacement parameters are normally refined for nearly all atoms (exceptions are very light atoms). Due to intrinsic characteristics of the refinement process, which will not be explained here, the displacement parameters are very sensitive to systematic errors in the data set (absorption, extinction). Disorder in the structure or imprecise coordinates of the atoms are also reflected in the displacement parameters. Reasonable values for these parameters are therefore a good indication for the correctness of a structure determination.

The atomic scattering factor f is not only a function of the scattering angle 2Θ but also of the X-ray wavelength λ (figure 30). If the energy of the incoming beam is high enough to expel electrons from their energy levels around the atom, an instant decrease of scattering power occurs, similar to the 'resonance catastrophe' in mechanics. Resonance can occur between X-rays and the K, L and M levels of the atoms.

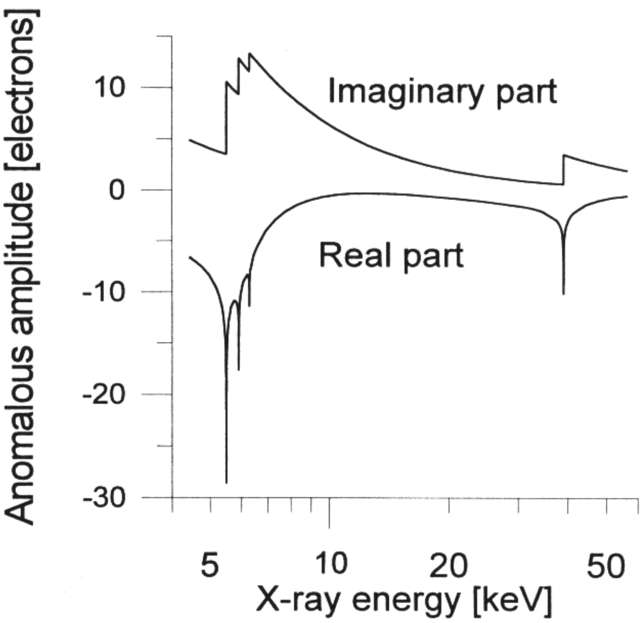

Fig 30: Variation of the anomalous scattering factors f' und f'' of Bi with X-ray energy.

As an approximation, the structure factor can be separated into the following components:

$$f_a(\Theta,\lambda)=f(\sin\Theta/\lambda)+f'(\lambda)+if''(\lambda) \qquad (10)$$

where f denotes the normal structure factor, whereas f' and f'' are named the real and the imaginary part of the anomalous scattering term. Numerical values for f' and f'' are available in Tables or on the WWW. The effect described here is utilized for the construction of filters (see chapter 3.1). A typical application for anomalous dispersion in diffraction methods is the increase of contrast for the form factors of elements with similar atomic number (i.e. Bi, Pb). This often allows an unambiguous identification of the element which occupies an atomic site.

7.2 The structure factor

The structure factor can be expressed as the Fourier sum over all atoms j in a unit cell,

$$F_{hkl}=\sum_{j=1}^{N} f_j \exp\left[2\pi i\left(hx_j+ky_j+lz_j\right)\right]=|F|\exp(i\phi) \qquad (11)$$

with the phase ϕ of the reflection. The intensity of a diffraction peak is proportional to the squared value of the structure factor (= multiplication of the structure factor by its conjugate complex).

$$I \approx |F_{hkl}|^2=\left(\sum_{j=1}^{N}\left(f_j\cos 2\pi(hx_j+ky_j+lz_j)\right)\right)^2+\left(\sum_{j=1}^{N}\left(f_j\sin 2\pi(hx_j+ky_j+lz_j)\right)\right)^2 \qquad (12)$$

Because of the squaring, the differences in scattering power of the atoms are magnified, which has important consequences. Thus if heavy atoms are present in the crystal structure, the phases of diffraction peaks are mainly determined by these strong scatterers and the determination of the positions of light atoms is in this case of limited precision.

Equation 12 clearly shows that the intensities do not contain any direct information about the phases of the structure factors, which are needed to reconstruct the electron density.

$$\rho(x,y,z)=\frac{1}{V_0}\cdot\sum_{h=-\infty}^{\infty}\sum_{k=-\infty}^{\infty}\sum_{l=-\infty}^{\infty}F_{hkl}\exp(-2\pi i(hx+ky+lz)) \qquad (13)$$

This is known as the phase problem in crystallography and its solution is the challenge in every structure determination. For a centrosymmetric structure, the sine term of equation 13 vanishes and the values of the phases are restricted to 0 and 180º. If a sufficient number of individual intensities of Bragg reflections are measured, the phases can usually be reconstructed using e.g. Direct Methods or the Patterson function (see chapter 9).

7.3 Intensity corrections

When the intensities are extracted from a single crystal or powder diffraction pattern, several systematic errors have to be taken into account and the intensities have to be corrected accordingly. In the following a brief overview of the most important corrections applied will be given.

7.3.1 Polarization correction

The oscillation of electrons is only possible perpendicular to the beam direction. Therefore, the component of the oscillation vector in the plane of incoming and diffracted beam is decreasing with increasing diffraction angle 2Θ and a correction for this effect is indispensable.

7.3.2 Lorentz factor

Diffraction arises when a reciprocal lattice node crosses the Ewald sphere. This node has a non-negligible volume and remains in diffraction position for some time. The intensity is of course proportional to the time that the lattice node remains on the Ewald sphere. The so-called Lorentz factor takes this effect into account and corrects for it.

7.3.3 Absorption factor

Absorption of X-rays in a crystalline material decreases the intensity depending on the length of the path through the sample. The intensity of the diffracted X-rays is thus reduced by the factor

$$I / I_0 = e^{-\mu x} \qquad (14)$$

where x is the total pathlength and μ is the linear absorption coefficient of the material.

7.3.4 Warming up process of the X-ray generator

Among others factors influencing the intensity of a diffraction pattern, it is crucial to know about systematic errors which are due to the diffractometer. It is good practice to wait at last for 12 hours after turning on the X-ray tube to full power, before a measurement is started as during the warming up phase, intensity changes of more than 15% can occur.

7.3.5 Overspill effect (specific for powders)

In flat plate powder diffraction geometry, it frequently happens that the X-ray beam spills over the sample at low diffraction angles 2Θ which causes an underestimation of peak intensities (figure 31).

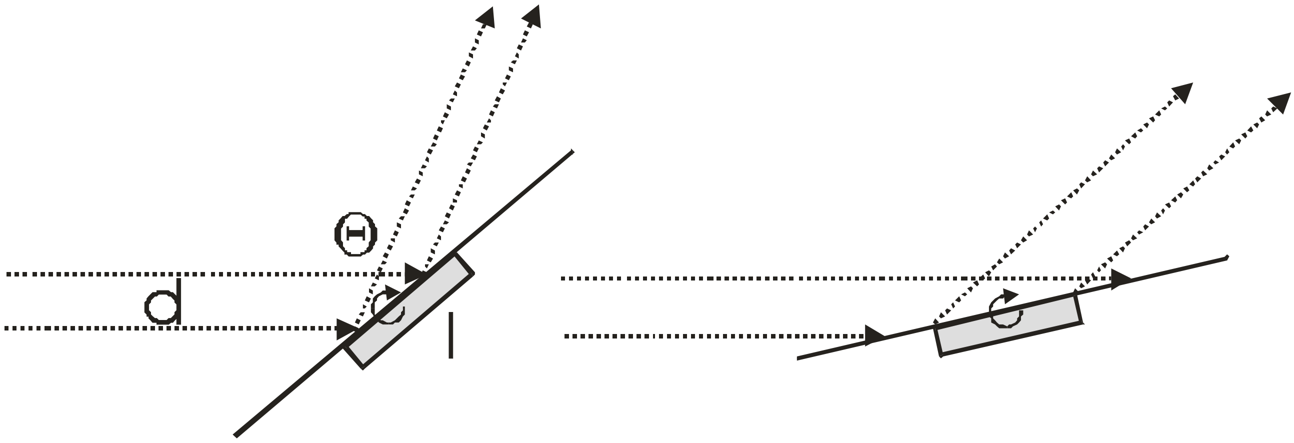

Figure 31: Overspill effect for flat plate samples in parallel beam geometry with the thickness of the beam d, and the length of the sample l.

7.3.6 Grain size effects (specific for powders)

The effect of the grain size on a powder diffraction pattern can be easily understood using a two dimensional example. Let’s assume a 2D single crystal in an arbitrary orientation and its 2D diffraction pattern (figure 32).

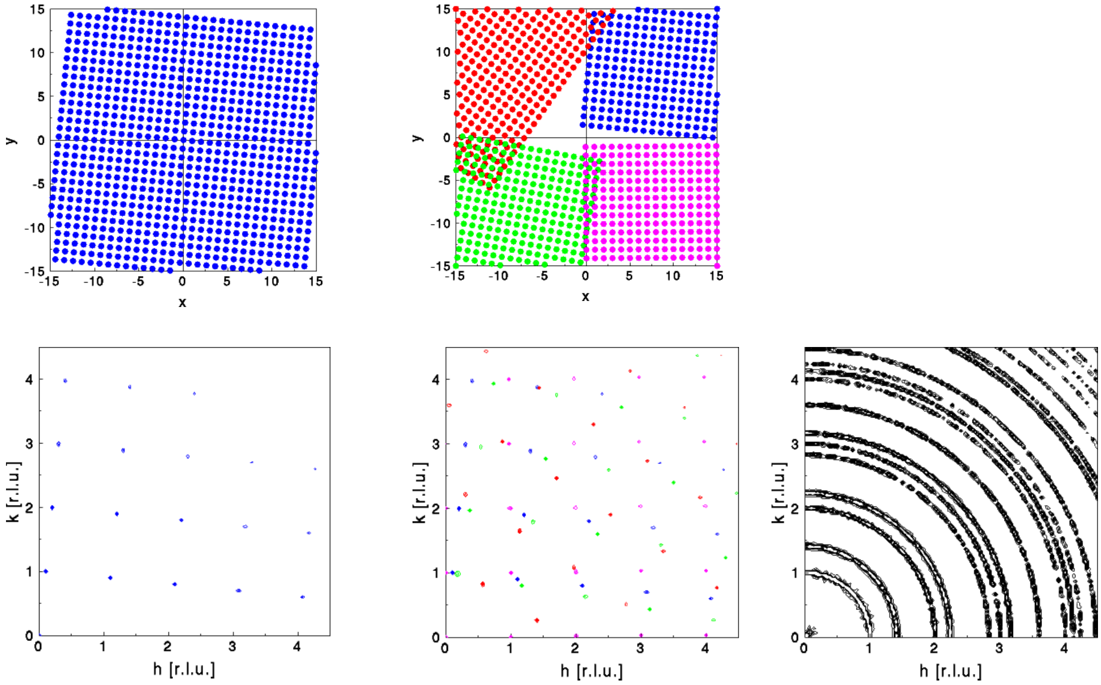

Figure 32: One, four and a large number of 2D- single crystals in random orientation and their corresponding diffraction pattern below.

If the number of crystallites in random orientation increases the diffraction patterns are superimposed and form one or more arcs depending on the orientation of the crystallites. In case of a ‘real’ powder with several million grains, the points degenerate to uniform rings in 2D and uniform cones in the 3-dimensional case. In an ‘ideal’ powder without preferred orientation, the diffracted information at each point of the Debye-Scherrer cone is identical and it is sufficient to scan the diffraction cones equatorially with a one-dimensional detector (i.e. scintillation counter). If, on the other hand, the powder consists only of very few grains or if the individual grains are too large, the rings recorded with an area detector (i.e. image plate system) become spotty and it is clear that a simple equatorial scan would result in meaningless intensities.

7.3.7 Multiplicity factor (specific for powders)

The multiplicity M stands for the number of reflections of a face set $\{hkl\}$, which have identical *d*-spacings and therefore overlap systematically in a powder diffraction pattern (i.e. in case of a cube, $\{100\} \equiv (100),(\bar{1}00),(010),(0\bar{1}0),(001),(00\bar{1})$). Depending on the crystal system, M can take values from 2 to 48. Values for M can be found in the International Tables of Crystallography.

7.3.8 Preferred orientation (specific for powders)

Grains in a powder are often not spherical but needle- or platelike depending on the preferred cleavage of the crystals. Therefore in a powder sample for flat plate geometry (reflection geometry), there will be no equal distribution of all orientations in space but one or more preferred orientation(s) are frequently encountered. This leads to an increase of the intensities of all those reflections with plane vectors (hkl) similar to that of the preferred orientation(s).

8 The profile of a Bragg reflection

In single crystal diffraction the correct treatment of the peak profile naturally plays an important role to extract good correct integrated intensities; yet in powder diffraction the correct treatment of the profiles is of vital importance for the successful solution and refinement of the structure and therefore some details about this subject will be given in the following.

The profile of a powder diffraction peak consists of three parts: the background B, the integrated intensity of the reflection I and the profile of the reflection, which can be regarded as a folding (*) of the spectral distribution of the X-ray radiation *W* with the instrument *G* (instrumental broadening) and the real structure of the sample (sample broadening) like grain size and lattice strain (figure 33).

$$F(2\Theta) = I \cdot ((W * G) * S) + B \qquad (15)$$

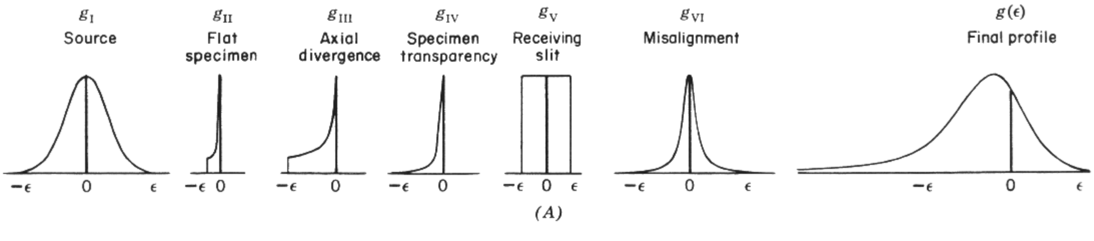

Figure 33 Contributions of instrumental components to the profile of a powder diffraction peak.

The determination of the pure sample related components of the peak profile is possible by Fourier transformation of the function which can be obtained by dividing the background corrected and Fourier transformed function *F* by the product of the Fourier transformed functions *W* and *G*. This method is time consuming and requires the prior knowledge of *W* and *G* or *W**G*, which is seldom available. An experimental determination of *W**G* is only possible, if a sample completely free of sample broadening has been measured. Strictly speaking such a sample does not exist but for daily work, the NBS peak profile standard lanthanum heaxaboride (LaB_6) can be used.

A flexible and physically meaningful description of the profile function of a powder diffraction peak is crucial for the precise determination of peak parameters like the position, the full width at half maximum (FWHM) and the intensity. This is particularly important for strongly overlapping reflections where the distance between consecutive diffraction peaks is less than 50% of their FWHM. Especially for intensity extraction from single peak or whole powder pattern fitting the selection of the 'correct' peak profile function mainly determines the quality of the result.

8.1 The (pseudo-)Voigt function

If all geometrical and physical properties of the X-ray source, the diffractometer and the sample were known, it would be straightforward to calculate the peak profile function. Yet in practice the realization of such a „fundamental parameter profile fitting procedure“ is quite complicated and not completely elaborated. In daily work, semi-empirical functions are used, which describe the entire profile of a powder pattern using only very few refinable and physically meaningful parameters. Since most contributions to the line profile can somehow be related to Lorentz- (i.e. Darwin profile) or Gauss- functions (i.e. crystallite size & micro strain), a 'mixture' between Gauss and Lorentz distribution (figure 34) is often used, the so called pseudo-Voigt function.

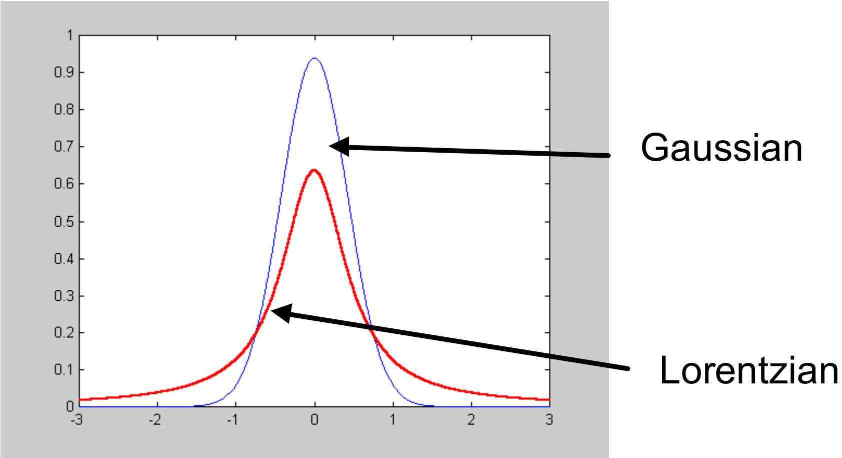

Figure 34 Schematic drawing of a Gauss and a Lorentz distribution.

8.2 Asymmetry due to axial divergence

Powder diffraction peaks usually show a certain asymmetry, which is predominantly caused by axial divergence (figure. 35).

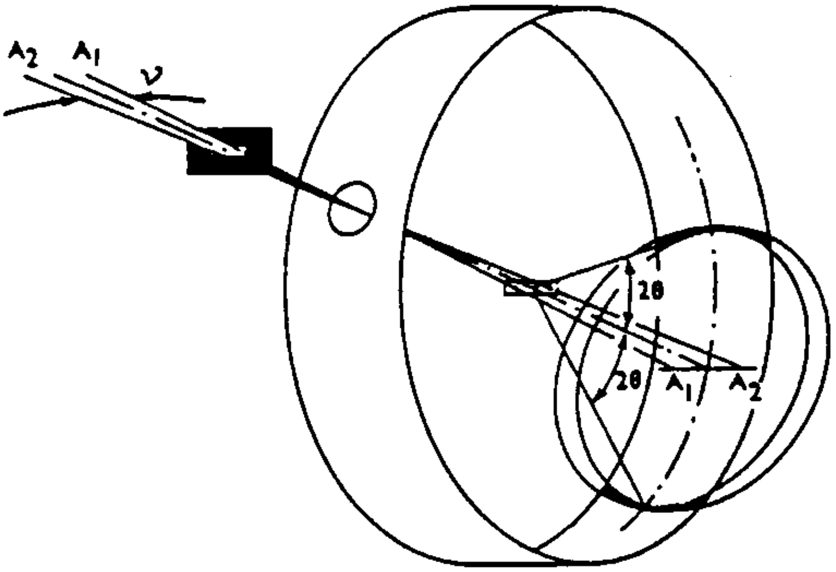

Figure 35: Asymmetric broadening of powder diffraction peaks due to axial divergence in Debye-Scherrer geometry using a divergent beam from a laboratory source.

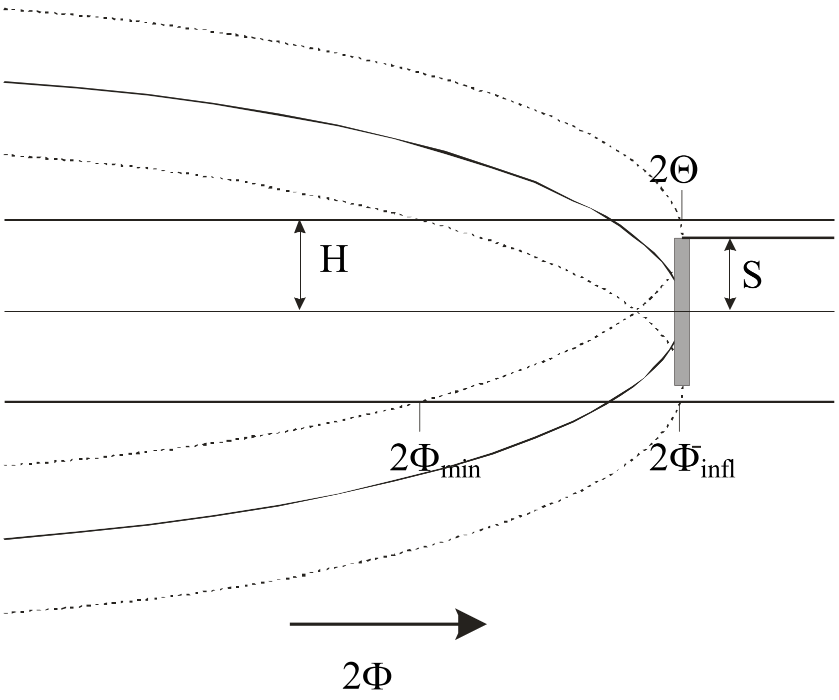

Figure 36: Schematic drawing of axial divergence. The half-axes of the ellipsoids are exchanged for clarity In the range $2\Phi>2\Theta$ *and* $2\Phi<2\Phi_{min}$ *no intensity will be detected; up to the angle* $2\Phi_{infl}$ *the amount of sample as seen by the detector increases.*

Axial divergence can be explained as follows: The diffracted radiation in X-ray powder diffraction is distributed over cones (Debye-Scherrer cones) with opening angle 4Θ. The receiving slit of the detector is located on the surface of a cylinder of radius L (= distance between sample and detector. The intersection of the diffraction cone and the surface of the cylinder are ellipsoids. Since the height of the receiving slit is 2H, only those segments of the ellipsoids will be measured which are located on a band of height 2H. The smaller the diffraction angle, the smaller is the radius of the diffraction cones and the larger is the bending of the ellipsoids and therefore the asymmetry of the recorded diffraction peaks. The asymmetry is further increased by the height 2S of the sample, which causes additional diffraction cones with axes above and below the central cone (figure 36).

8.3 Sample broadening

8.3.1 Crystallite size

According to Scherrer, it is possible to determine the average grain size of spherical crystallites by measuring the FWHM of the diffraction peaks corrected for the contributions from the diffractometer. The thickness of a crystallite consisting of p lattice planes of thickness d calculates to $L_{hkl} = p \cdot d$. The relation between L_{hkl} and the FWHM of the diffraction peak (hkl) can directly be derived from the Bragg equation

$$\beta_{hkl} = 4\varepsilon_{1/2} = \frac{4 \cdot 1.4\lambda}{2\pi p d \cos\Theta} = \frac{0.89\lambda}{L_{hkl}\cos\Theta} \tag{14}$$

With the average grain size L_{hkl} of a powder (for grain sizes below 0.1 μ(= 1000Å)) and the FWHM β_{hkl} in radians.

8.3.2 Lattice strain

Strain in a crystal lattice is a distribution of lattice parameters around an average value caused by defects, not by an external force (figure 37). A sample with isotropic strain produces peak broadening in reciprocal space which is augmenting with increasing distance of the reflections from the origin (figure 37).

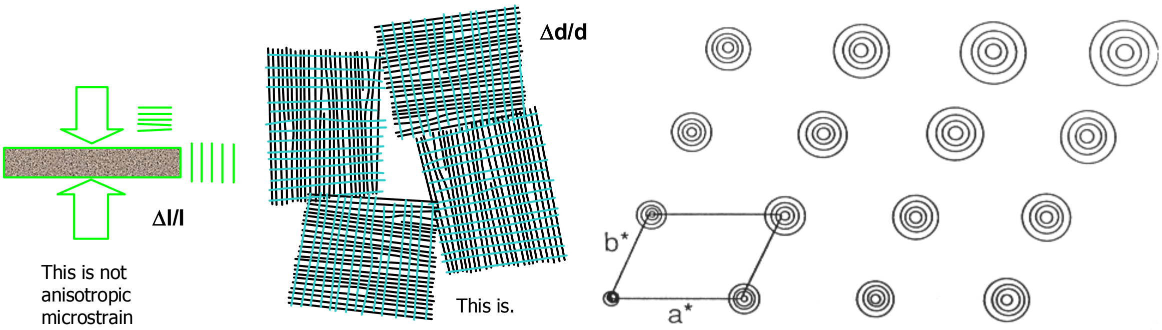

Figure 37: Left: schematic drawing of the difference between strain induced by external forces and internal lattice strain due to defects in the crystal structure. Right: schematic drawing of peak broadening in reciprocal space due to lattice strain.

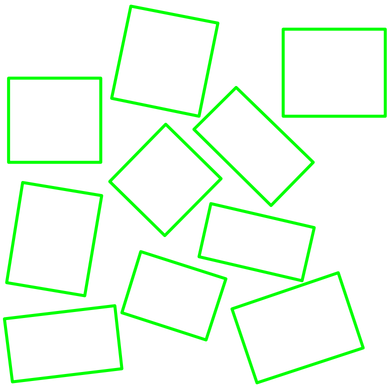

Each grain is described by a particular set of lattice parameters, {*a, b, c,* α, β, γ}, so there could be a 6-dimensional distribution of these metrics, deviating from their average values.

(*a* and *b* have negative correlation, γ ≡ 90)

Figure 38: Schematic drawing of a distribution of lattice parameters for an assembly of grains.

The Bragg equation (equation 5) directly relates the broadening Γ of a Bragg reflection to (uniform) lattice strain:

$$\frac{\partial d}{d} = \Gamma \tan \Theta^{-1} \qquad (15)$$

If d^*_{hkl} is the inverse of the lattice plane distance d of the reflection (hkl), then d^{*2} is bilinear in the Miller indices and can be developed in expressions which have a relation to the covariances of the lattice parameter distribution. Each crystallite is considered to have its own set of lattice parameters which are different from the average values (figure 38). This leads to a multidimensional distribution of lattice parameters over the entire powder sample. The width of each diffraction peak can be expressed by the moments of this distribution. This leads to an expression for the anisotropic broadening Γ_A in which the variance of d^{*2} is equivalent to a sum of 15 different combinations of Miller indices up to the fourth order:

$$\begin{aligned} \Gamma_A^2 = [&S_{400}h^4 + S_{040}k^4 + S_{004}l^4 + 3(S_{220}h^2k^2 + S_{202}h^2l^2 + S_{022}k^2l^2) \\ &+ 2(S_{301}h^3l + S_{103}hl^3 + S_{031}k^3l + S_{130}hk^3 + S_{301}h^3l + S_{013}kl^3) \\ &+ 3(S_{211}h^2kl + S_{121}hk^2l + S_{112}hkl^2)]d^{*4}_{hkl} \tan^2\Theta \end{aligned} \qquad (16)$$

In the profile fitting process, the parameters S_{hkl} are refinable. The number of parameters varies due to symmetry restrictions from 15 in the triclinic to only 2 in the cubic crystal system. The anisotropic contribution to the peak broadening of a powder diffraction peak is given (in radians) by

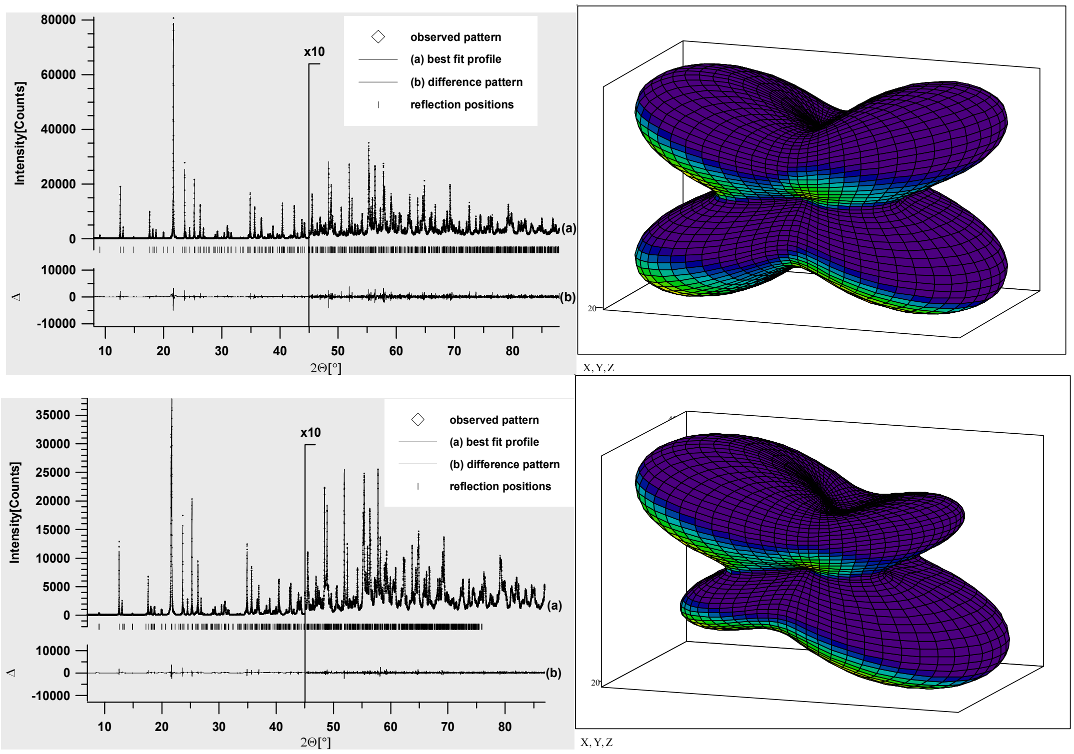

Figure 39: LeBail fit and microstrain distribution of the orthorhombic high temperature phase (295 K, top) and the monoclinic low temperature phase (50 K, bottom) of Bi_2CdGeO_6.

It is important to note that anisotropic peak broadening due to lattice strain contains gaussian as well as lorentzian components, which therefore must be refined simultaneously in order to achieve a good fit to the powder diffraction pattern. This is achieved by introducing a mixing parameter ζ to the anisotropic extension of the Gauss part of the FWHM distribution

$$\Gamma_G = (U\tan^2\Theta + V\tan\Theta + W + (1-\varsigma)^2\Gamma_A^2(hkl))^{1/2} \qquad (17)$$

and of the lorentzian part of the FWHM distribution

$$\Gamma_L = X\tan\Theta + Y/\cos\Theta + \varsigma\Gamma_A(hkl) \qquad (18)$$

in which U, V, W, X, Y denote refinable parameters. The obvious advantage of a physically meaningful description of anisotropic peak broadening is a better Rietveld refinement which yields more structural details (in special cases even the determination of hydrogen atom positions). In addition, phase transitions with large hysterisis are sometimes easier to detect by the analysis of the microstrain distribution than by refining lattice parameters (e.g. if a monoclinic angle is very close to 90.0°). An illustrative example are the high and low temperature phases of the ternary compound Bi_2CdGeO_6 (figure 39).

9 Crystal structure solution

9.1 The Patterson function

Two substantially different approaches are used in crystallography to solve the phase problem. While one tries to determine the phases of the reflections directly (direct methods) by using statistical methods, the other makes use of the so-called Patterson function which can be calculated from the experimental intensities. In general lines Patterson methods are successful whenever one or few heavy atoms are found within a structure, while Direct Methods work the better the more similar the atomic species. Normally one of the two methods yields the solution of the phase problem, yet there are still some cases where the solution can be hard or even impossible to find.

The solution of the phase problem is practically identical with the determination of the coordinates of the atoms. Thus, the appliance of Patterson or Direct Methods yields a more or less sophisticated model which contains the coordinates of a fraction of the atoms within the structure. The subsequent use of refinement programs in combination with difference Fourier synthesis (see chapter 10.1) leads to the final results.

Patterson suggested in 1935 to use the function which was afterwards named after him as an aid for the solution of the phase problem. The Patterson performs a Fourier transformation of the squared absolute values of the structure factors and is defined as :

$$P(r) = 1/V\, |F_{\mathrm{H}}|^2\, exp(-2\pi\, H\, r) \qquad (19)$$

With $r = xa + yb + zc$ as a position in the unit cell space and $H = hx + ky + lz$ as a lattice point in reciprocal space. Mathematically the Patterson function is a self convolution of the electronic density function $\rho(r)$. The Patterson function is a real function and therefore the above equation simplifies to:

$$P (r) = 1/\mathrm{V} \sum_{\mathrm{h}}\sum_{\mathrm{k}}\sum_{\mathrm{l}} |\mathrm{F}_{\mathrm{H}}|^2 \;\cos 2\, \pi(hu + kv + lw) \qquad (20)$$

The function has n (n-1) peaks (neglecting the origin peak) if there are n-atoms in the unit cell. These maxima correspond to the interatomic vectors in the crystal structure. The height of these maxima is given by the product of the atomic numbers of the two atoms concerned multiplied by the multiciplicity of the interatomic vector.

The Patterson function can be easily calculated from the experimental data as the $|F_{\mathrm{H}}|^2$ values follow directly from the experiment. The difficulty is the interpretation of the calculated map in which one has to recognize the repeated configuration of maxima corresponding to molecules or coordinated complex groups. Several strategies which are employed in the practice for the solution of crystal structures follow straightforwardly from the Patterson method.

The so-called **heavy atom method** makes use of the fact that one or few heavy atoms within a crystal structure which is mainly composed of light atoms will produce high maxima in the Patterson map, making it easy to identify the corresponding interatomic vector and to determine the heavy atom positions. Once these positions are obtained as a starting model the rest of the structure is generally simple to determine via refinement and difference Fourier methods.

Other methods employed to interpret the Patterson map are the so-called **vector methods**. Here the **superposition method** is no doubt of special importance. In this procedure a Patterson map is superimposed on itself with a displacement vector which is chosen from the map and has to coincide with an interatomic vector of the real structure to obtain a suitable solution. In the two superimposed maps the set of coincident peaks reveals one or more images of the structure. If just one image is produced the solution is straightforward. If a multiple image is produced the process is repeated with an additional superposition vector.

The problem of the superposition method is that it works well for Patterson functions of theoretical point atom structures but in practice the function is continuous and it is not trivial to evaluate the degree of coincidence between the peaks of superimposing maps. To overcome this difficulty the so-called **image seeking functions** are employed.

Additional methods mainly used in combination with Patterson methods are the **isomorphous** or **molecular replacement methods** and the determination of crystal structures using the effect of **anomalous dispersion**. The latter makes use of the fact that the scattering power of an atomic species changes abruptly at its absorption edge and consequently the heights of the peaks in a Patterson map change. By evaluating the differences in the Patterson maps calculated with data measured at two different wavelengths (close to and far away from the absorption edge), it is possible to draw conclusions of the type and position of the atomic species in question.

The **Patterson search method** was especially developed for powder data. It is based on the fact that molecular fragments of known geometry have a particular set of interatomic vectors. This set of vectors can be rotated and translated until it fits into the Patterson map.

Summarizing the above it is evident that the Patterson method is extremely valuable to solve structures which contain one or few heavy atoms and in this case normally is the method of choice for structure solution. Yet also for structures containing geometric molecules which are characterized by a set of parallel vectors, the superimposing of all the parallel vectors in the Patterson map will lead to high maxima and the solution can be straightforward.

9.2 Direct Methods.

Direct Methods try to derive the structure factor phases directly from the observed F_{hkl} using mathematical relationships. Two important properties of the electron density function form the basics of Direct Methods. Firstly the electron density is always positive and secondly it is composed of discrete atoms. Since the establishment of the first mathematical relationship between the phases in 1948 by Harker & Kaspar, Direct Methods have developed rapidly and a lot of specialized literature on the subject is available. Here we will therefore concentrate on the principal ideas.

Direct Methods basically comprise the following steps:

1. Normalization of the structure factors

The normalization of the structure factors takes into account the decrease of the scattering power with Θ. The normalized structure factors E_H simulate a structure with point-like atoms, the scattering power of which does not depend on Θ

2. Fixing the Origin

While $|F_H|$ and $|E_H|$ depend only on the distribution of the atoms in the unit cell the phase is also dependent on the selection of the origin i.e. the phase changes when the origin of the crystal structure is changed. To fix the origin suitable reflections (generally with large $|E_H|$ values) are chosen and their phase is fixed.

3. Establish relationships between the normalized structure factors

By far the most important relationship used for phasing in direct methods is the so called triple product or $\sum_2$ -relationship which is based on the equation of Sayre:

$$F_H = \Theta_H / V \sum_{H'} F_{H'} F_{H-H'} \qquad (21)$$

From this equation follows the $\sum_2$ –relationship

$$E_H = \sum_{H'} E_{H'} E_{H-H'} \qquad (22)$$

This means that the phase of E_H is determined by the phases of $E_{H'}$ and $E_{H-H'}$. Figure 40 illustrates the relationship which is described by this equation. If the electron density is concentrated around the regions A,B,C,D then the amplitudes of the three structure factors are large. Solid and dashed lines represent positive and negative maxima respectively for the reflections. In each case the product of the three structure factors is positive. The $\sum_2$ condition establishes a relationship between the phases of three structure factors which is true with a certain probability.

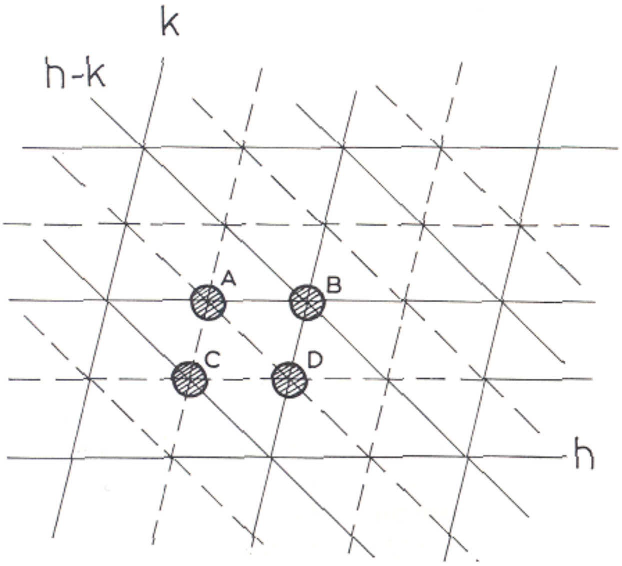

Figure 40: Large amplitudes for F_h, F_k and F_{h-k} are produced it the electron density is concentrated in the regions ABCD. The product of the three structure factors is always positive. Solid and dashed lines correspond to positive and negative maxima for the three reflections.

Other relationships between structure factors can also be established (e.g. $\sum_1$ relationship or negative and positive quartets). Expressions for the probabilities of the correctness of the relationships established between the phases can be found in literature.

4. Determine new phases/symbolic addition

Using the reflections that fix the origin and the corresponding phases, one searches all the possible triple products and in this way determines the phases of additional reflections. If not enough phases can be determined, more reflections are chosen, whose phases are represented by symbols. These symbolic phases are then also expanded (symbolic addition). Often relationships between the symbols are found in this process and the number of additional symbols can be reduced. If finally a certain number *p* of symbols is unknown the corresponding Fourier maps are calculated for all the possible combinations symbol/phase and ensuing maxima are interpreted.

5. Seeking the right solution from a series of suggestions

The last step yields a set of possible solutions for the structure. For each of them figures of merit (e.g. weighted sums between calculated and observed structure factors) can be calculated and generally the identification of the right solution is straightforward.

9.3 Specialized methods for powder diffraction

In a powder pattern information is lost due to the projection of the 3-dimensional reciprocal space on a 1-dimensional $|\vec{Q}|$ axis, which results in systematic and/or accidental overlap of reflections.

Therefore, all structure solving methods which rely on the exact determination of individual peak intensities are limited to either very high resolution powder diffraction data or relatively small crystal structures.

In general, the common structure determination algorithms can be divided in two major categories. The first group is called ‘classical’ methods and uses the algorithms which have been developed for the structure determination of single crystals (see chapters 9.1 and 9.2) and then have been modified to satisfy the needs of powder diffraction data. These classical methods rely on the precise determination of individual peak intensities. Therefore the strong overlapping of reflections in a powder pattern limits the complexity of crystal structures which can be solved with these methods. The use of high resolution synchrotron radiation or the improved extraction of peak intensities has extended this limit. Furthermore, iterative algorithms can be used to improve the derived structure information by recycling the extracted peak intensities and vice versa.

The second group of methods – the so-called direct space methods - were developed recently and work in a completely different manner. Here, the structural model is first postulated independently of the powder diffraction data. From this model, either individual Bragg intensities or the entire powder pattern is calculated and then compared with the observed data. Improvement of the model can then be achieved in various ways using energy minimization, global optimization or a simple grid search. The basic requirement of these methods is the prior knowledge of the connectivity of the atoms and the kind and number of degrees of freedom which is normally known for molecular crystal structures.

Grid search in crystal (direct) space

During a grid search the degrees of freedom (translation, rotation, torsion etc.) of structural fragments are varied systematically in the unit cell. To improve the simulated model, the sum of the differences between observed and calculated structure factors and/or powder patterns is minimized. It is often possible to limit the degrees of freedom using chemical knowledge (e.g. short distances between neighbor molecules, ranges for torsion angles, chain lengths etc.).

Method of Maximum Entropy (MEM) and likelihood ranking

The method of maximum entropy (MEM) enables the calculation of high quality electron density maps and ideally enables direct phasing. Starting from an initial electron density which is equally distributed over the unit cell volume, the most probable electron density is calculated step by step using an iterative procedure. Likelihood ranking indicates the way of growing of a phasing tree with which the most probable phases of Bragg reflections will be determined.

Monte-Carlo methods and simulated-annealing

These methods are based on the same principle as a grid search, but each variation of the trial structure is based on the previous variation. Within certain limits, the variations are random. The different algorithms differ in the way of their acceptance criterion for variations. In the case of simulated annealing, variations which lead to a worsening of the agreement factor are also accepted with a certain probability which is reduced during the structure determination process. This trick allows jumping out of local minima to ensure proper sampling of crystal space.

Lattice energy minimization (molecular modeling)

The sum of the electrostatic and the Van-der-Waals interactions between molecules is minimized in addition or independent to the information of a powder diffraction pattern. starting from random packing of the molecules. This can be done by grid search and/or least squares methods.

Genetic algorithms

The principle of genetic algorithms is based on the Monte Carlo procedure, whereas the variation of the structural model is performed according to the principles of genetics. Modified models which have ‘survived’ are crossed and mutated in order to form new ‘populations’ of which the ‘weak members’ are sorted out after a test.

Periodic nodal surface (structure-envelope)
A few Bragg peaks at low diffraction angle with known phases are enough to split the unit cell into regions of high and low electron density. This information can be used as a geometric restriction for a grid search.

Pseudo-atom-method
More or less cyclic molecular fragments can be substituted by the sum of spherical shell form factors. Using grid-search techniques and Rietveld refinement it is possible to determine the centers of gravity of these fragments. The missing orientation of the molecular fragments can then be determined by a grid search after back-substitution. This procedure drastically reduces the number of degrees of freedom at the beginning of a crystal structure determination.

In case of powder diffraction, *Direct Methods* are mainly used for the determination of inorganic crystal structures, whereas global optimization methods in real space like *simulated annealing* are applied to molecular structures.

10 Crystal structure refinement

The partial solution of the crystal structure yielded by any of the above described methods must usually be completed by a combination of least-squares refinement and difference Fourier synthesis.
For the explanation of the least-squares refinement strategy one assumes an error free set of observed structure factors and an almost correct set of atomic coordinates and displacement parameters. For simplicity a centrosymmetric structure and isotropic displacement parameters

are considered. The structure factors calculated from the model are:

$$(F_c)_H = \sum_{j=1}^{N/2} 2 f_j \exp(-B_j \frac{\sin^2\theta}{\lambda^2}) \cos 2\pi (hx_j + ky_j + lz_j) \tag{23}$$

The correct parameters for the j-th atom can then be expressed as $B_j+\Delta B_j$, $x_j+\Delta x_j$, $y_j+\Delta y_j$, $z_j+\Delta z_j$ and one can write:

$$(F_o)_H = \sum_{j=1}^{N/2} 2 f_j \exp\left\{-(B_j + \Delta B_j)\frac{\sin^2\theta}{\lambda}\right\} \cos 2\pi \{h(x_j + \Delta x_j) + k(y_j + \Delta y_j) + l(z_j + \Delta z_j)\} \tag{24}$$

If the errors in the parameters are small one can write

$$(F_o)_H - (F_c)_H = \Delta F_H$$

$$\Delta F_H = \sum_{j=1}^{N/2} \frac{\partial (F_c)_H}{\partial B_j}\Delta B_j + \frac{\partial (F_c)_H}{\partial x_j}\Delta x_j + \frac{\partial (F_c)_H}{\partial y_j}\Delta y_j + \frac{\partial (F_c)_H}{\partial z_j}\Delta z_j \tag{25}$$

An equation of this type can be produced for every reflection *H* and in general there are more equations of this type than refinable parameters. The least square solution for the set of equation is such that the quantity

$$R = \sum_H \{(F_o)_H - (F_c)_H\} \tag{26}$$

is a minimum.

If one takes into account that the observed structure factors have different experimental errors, it is reasonable to weight the above mentioned equations according to the expected reliability of the quantity ΔF_H. Different weighting schemes are employed in structure refinement.

10.1 Difference Fourier synthesis

Normally the model from the structure solution does not yield the position of all the atoms in the structure. To complete and refine the structural model further, difference Fourier synthesis is widely used. For this a Fourier series of the type

$$\Delta\rho(r) = \frac{1}{V}\sum_{H}\left(\left|F_H^o\right| - \left|F_H^c\right|\right)\exp(-2\pi Hr + i\varphi_H^c) \qquad (27)$$

is employed. If in the model an atom is missing $\rho^{calc}(r)$ is zero while $\rho^{obs}(r)$ shows a maximum. Therefore $\Delta\rho(r)$ also shows a maximum. Similarly other errors in the model like errors in the atomic positions or in the displacement parameters give rise to maxima in the function $\Delta\ \rho(r)$.

10.2 Powder Pattern Profile Fitting

10.2.1 The Rietveld Method

The Rietveld method is considered a milestone in structure refinement from powder diffraction data. The basic idea behind the Rietveld method is the calculation of the entire powder pattern using a variety of different refinable parameters. The calculated intensity $y_i(calc)$ for a mixture of phases

$$y_i(calc) = \sum_{p}\left(S_p \cdot \sum_{pH}\left(M_{pH} \cdot A_{pH}(2\Theta_i) \cdot P_{pH} \cdot \left|F_{pH}(calc)\right|^2 \cdot LP(2\Theta_i) \cdot \Phi_{pH}(2\Theta_i)\right)\right) + B_i(obs) \qquad (28)$$

at point i of the powder pattern is calculated from the contributions of all phases p contributing to the powder pattern and all Bragg reflections H of phase p, with the scale factor S_p, the multiplicity M_{pH}, the absorption correction $A_{pH}(2\Theta_i)$, the preferred orientation correction P_{pH}, the squared absolute value of the structure factor $\left|F_{pH}(calc)\right|^2$, the Lorentz-Polarization correction $LP(2\Theta_i)$, the normalized profile function $\Phi_{pH}(2\Theta_i)$ and the background contribution $B_i(obs)$.

The parameters can roughly be divided into three categories: *structural* parameters, which mainly affect the intensities of the Bragg reflections, *profile* parameters, which are determined by the instrument and the sample, and *background* parameters. For the calculation of any single point i in the powder pattern, all reflections H contributing to this point as well as the height of the background $B_i(obs)$ must be taken into account. The scale factor S_p is used for quantitative phase analysis, the intensity $\left|F_{pH}(calc)\right|^2$ for refinement of the crystal structure and the profile function $\Phi_{pH}(2\Theta_i)$ for the refinement of the microstructure (microstrain, domain size).

The weighted sum of the squared differences between the observed and the calculated powder pattern is minimized by refining a selection of parameters using least squares methods.

$$\sum_i w_i\left(y_i(obs) - y_i(calc)\right) \rightarrow Min, w_i = \frac{1}{\sqrt{y_i(obs)}} \qquad (29)$$

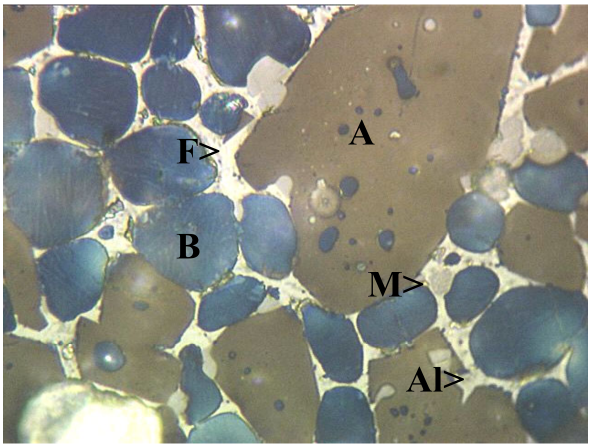

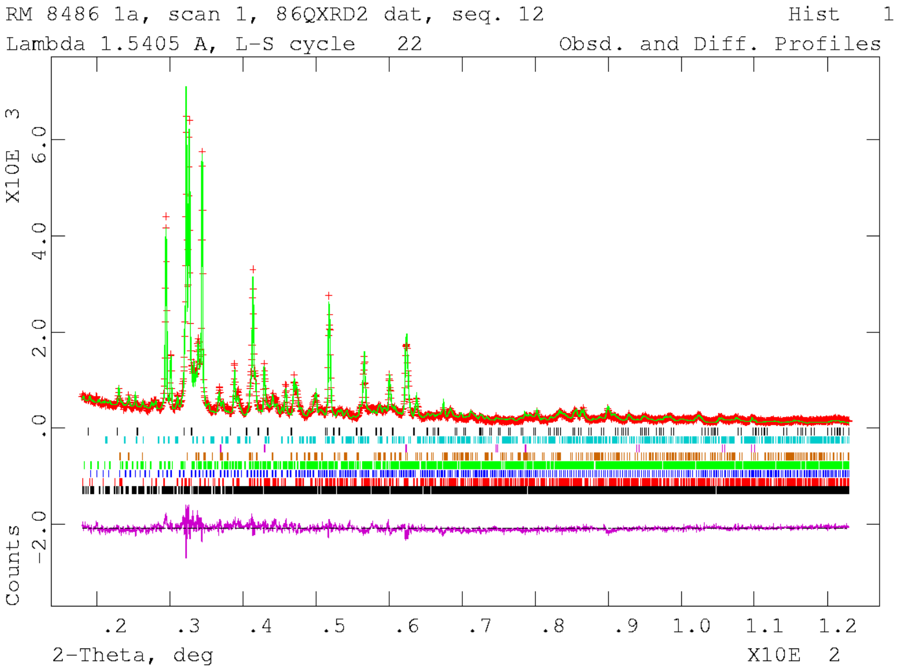

Figure 41: Reflected light micrograph (field width: 250 mm) of RM 8486 cement clinker (top) containing alite (A), belite (B), ferrite (F), aluminate (Al), and periclase (M). and corresponding quantitative Rietveld refinement.

Many different statistical agreement factors have been proposed for judging the quality of a Rietveld refinement . The most common one is the so called weighted profile *R*-factor which is defines as

$$R_{wp} = \sqrt{\frac{\sum_i w_i \left(y_i(obs) - y_i(calc)\right)^2}{\sum_k w_i y_i(obs)^2}} \qquad (30)$$

The graphical representation of a Rietveld refinement, the 'Rietveld plot' shows the observed powder pattern, the best Rietveld fit profile, the reflection positions and the difference curve between observed and calculated profiles as the trace below. Due to the decrease of scattering power at higher diffraction angles, the high angle part is often enlarged.

The major advantage of the Rietveld refinement procedure is the iterative improvement of the structural information. On the other hand, a reasonably good structural model is required in advance to ensure the convergence of the refinement. Nowadays, even the Rietveld refinement of small protein structures from powder diffraction data is possible.

In the case of phase mixtures, the Rietveld technique can be used for ‘standardless’ quantitative phase analysis, provided the mass absorption coefficients of the phases are similar.

The performance of mixtures containing several (often polymorphic) phases like cement clinker is mainly governed by its mineralogy and not its absolute chemical composition. Since X-ray diffraction is related to the crystallographic structure of all phases present in a sample, XRD is the only tool for qualitative and quantitative analysis (figure 41).

The key problem in Rietveld analysis is the refinement strategy. In general, the profile, the background and the crystal structure parameters should be determined and refined separately in the beginning of the refinement. A typical strategy is to start with the refinement of the peak positions (lattice), followed by the profile parameters, the structural parameters, and finally the microstructure parameters like microstrain and domain size. Finally, all variable parameters should be refined simultaneously to obtain mathematically correct variances and covariances.

10.2.2 The LeBail Method

Nowadays, the LeBail-method is a widely used technique to refine the total envelope of a powder pattern without knowing the crystal structure and to extract intensities which can later be used for crystal structure determination by e.g. Direct Method programs. The basic idea used is relatively simple as the Le Bail method iterates the Rietveld decomposition formula. Where calculated structure factors $|F|$ are entered in the Rietveld decomposition formula a set of identical $|F|$ is given instead. The Rietveld refinement calculates a set of "$|F_{obs}|$" from the decomposition formula, which are then used as new $|F_{calc}|$ and so on.

10.2.3 The Pawley Method

Another widely used method which allows intensity extraction from powder diffraction data is the Pawley method, which basically is a full profile refinement. Besides the profile and lattice parameters all intensities are refined individually in the least squares process. Although this procedure is much slower than the LeBail method, it has a particular advantage for direct space methods on structure determination from powder diffraction data. The covariance matrix of the Pawley fit describes the degree of correlation between the individual intensities of neighboring reflections and can actively be used in the calculation of the level of agreement between the measured intensities and those of the trial structures in a global optimization process like simulated annealing.

11 Powder diffraction at non ambient conditions

11.1 Micro-Reactor

Many decomposition or solid-vapor reactions which are common in mineralogy cannot be fully understood due to the lack of structural information of the intermediate phases which often have a limited range of stability. A solution to this problem are powder diffraction measurements at reaction conditions using a micro reaction cell for *in situ* studies (figure 42), e.g. hydrothermal synthesis.

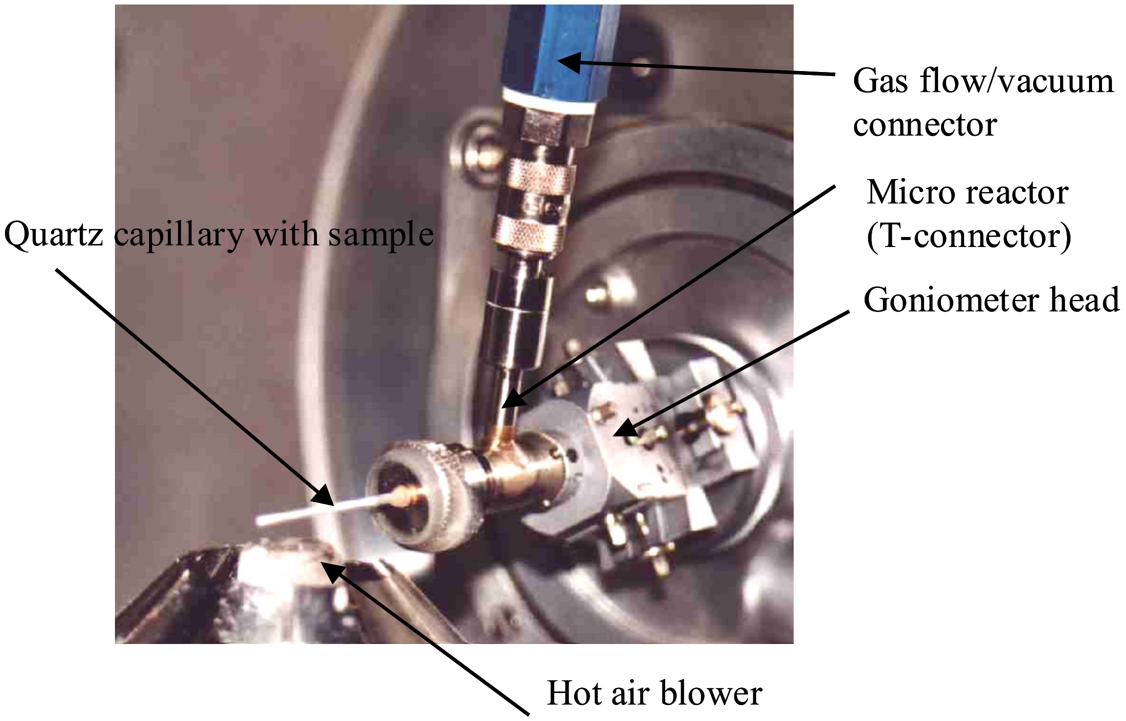

Figure 42: Micro reaction cell for in situ studies of hydrothermal synthesis at the high resolution powder X-ray beamline BM16 (ESRF).

A recent example is the investigation of the decomposition of silver carbonate, Ag_2CO_3, to metallic silver via silver oxide, Ag_2O. Before the decomposition of silver carbonate to silver oxide, two high temperature modifications of Ag_2CO_3 exist (α-Ag_2CO_3 and β-Ag_2CO_3) In order to determine the crystal structures of these high temperature phases it was necessary to stabilize the pure phases for prolonged periods of time, making it possible to collect high quality powder diffraction data at beamline BM16 at ESRF. The sample was kept under 4 atm. carbondioxide pressure in order to shift the decomposition to higher temperatures. The temperature was slowly raised and powder diffraction patterns of the different phases for structural analysis were collected (figure 43).

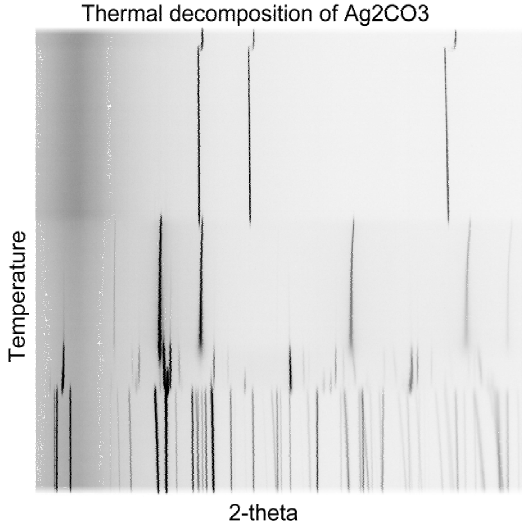

Figure 43: Translating Imaging Plate (TIP) Camera for Time Resolved Synchrotron X-ray Powder Diffraction

11.2 High Pressure Powder Diffraction

Diffraction studies at high pressures provide an opportunity to investigate the behavior of the chemical bonding of solids as a function of decreasing inter-atomic separation, without the complications introduced by changing chemistry. Using i*n situ* high pressure powder diffraction experiments the structural changes of minerals depending on pressure can be investigated and the pressure conditions of the earth mantle can be reproduced in the laboratory.

Figure 44: Selection of modern diamond anvil cells (DAC), available at beamline ID30 (ESRF)

In general, powder diffraction methods at high pressures yield data of lower quality than that which are obtainable at ambient conditions. When planning a X-ray powder diffraction experiment at high pressure, the angle dispersive technique at a third generation Synchrotron source is the method of choice. First of all, a suitable type of pressure cell must be chosen. For low pressures (up to 6 kbar), large volume gas pressure cells may be used. For higher pressures (up to the Mbar range), there exists a variety of different diamond anvil cells (DAC) (figure 44).

The diamonds are separated by a tungsten or steel gasket which must be pre-pressed in the empty DAC at moderate pressures and a hole of 0.1..0.2 mm diameter must be drilled. The sample is placed in the hole together with a (hydrostatic) pressure transmitting medium. Depending on the desired pressure range and the reactivity of the sample, different pressure media like silicon oil, ethanol-methanol mixture, nitrogen and argon are used. The pressure in the DAC will be measured using an internal pressure standard like quartz or externally by the ruby fluorescence method. A highly focused X-ray beam must be carefully aligned in order to avoid hitting the gasket. Due to the small amounts and the graininess of the samples, image plate detectors are widely used which allow the integration and averaging over the entire powder rings (figure 45). Recently, high pressure and low temperature experiments down to 10 K have been combined by placing the DAC into a cryostat. For high temperature annealing of samples in the DAC, a laser can be used. So called membrane DAC's allow *in situ* pressure variation.

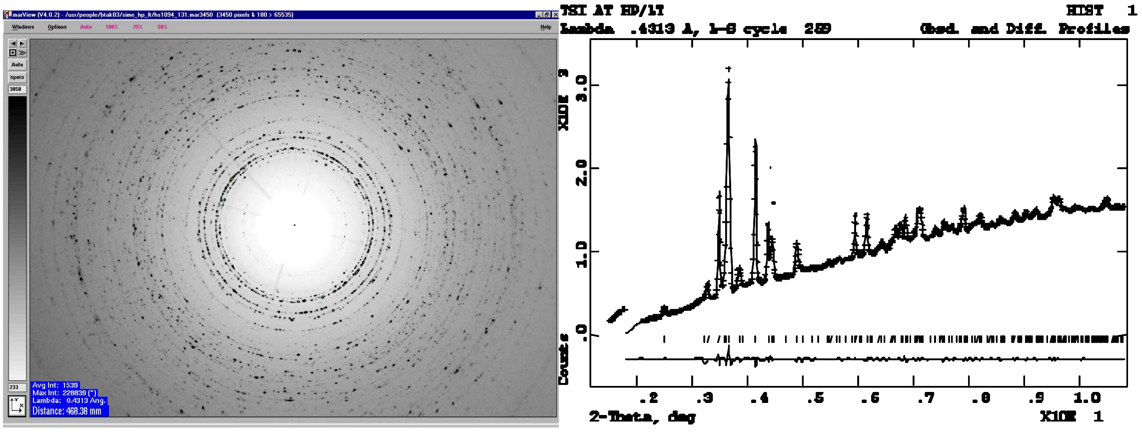

Figure 45: Image plate readout of a new recrystallized (note the 'spotty' circles) high pressure phase (left) and corresponding LeBail fit (right).

11.3 Energy Dependent Powder Diffraction

The free selection of the X-ray wavelength over a large energy range at the synchrotron enables so called depth profiling of polycrystalline layered samples due to the energy dependence of the penetration depth of the X-rays. An interesting application which demonstrates the usefulness of this method are plasma sprayed hydroxyapatite coatings which are used as bioactive surfaces for increasing the fixation of bones as dental implants or orthopaedic protheses. The variability in the performance of these coatings is partly attributed to the chemical phases which form at high temperatures in the plasma or alternatively to fast cooling rates upon deposition. Hydroxyapatite can be accompanied by an amorphous phase constituent, tricalcium phosphate, tetracalcium phosphate, calcium oxide or the rarely mentioned, oxyapatite.

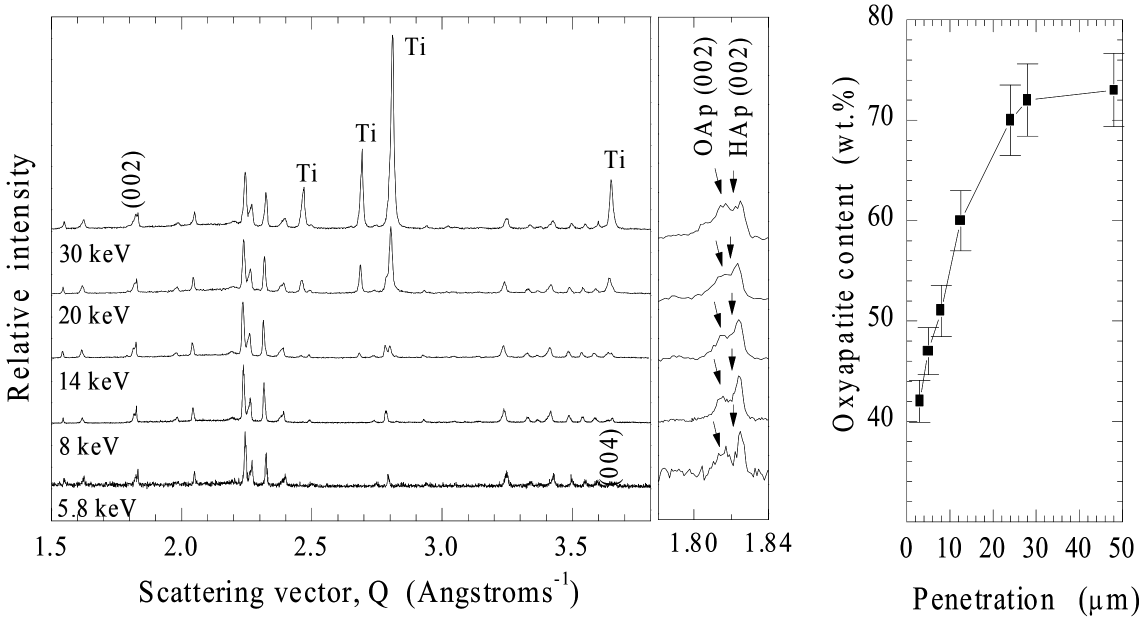

Figure 46. Detection of oxyapatite in X-ray diffraction patterns (left) and the amount of oxyapatite in proportion to both apatites (hydroxyapatite and oxyapatite) as a function of coating depth (right).

The high temperatures in the plasma produce a hydroxyl depleted layer on the outside of the traversing hydroxyapatite particle. It is this dehydroxylated area which may form oxyapatite upon deposition. Higher cooling rates produce an amorphous phase but a lower cooling rate will lead to the formation of oxyapatite. This presence and varying amounts of oxyapatite with coating thickness can influence the dissolution and mechanical performance of the coating for dental and orthopaedic prostheses.
Examination of the coating at various depths with X-ray diffraction reveals a higher oxyapatite content in the underlying layers (figure 46).

12 Texture, Stress and Microdiffraction

12.1 Texture

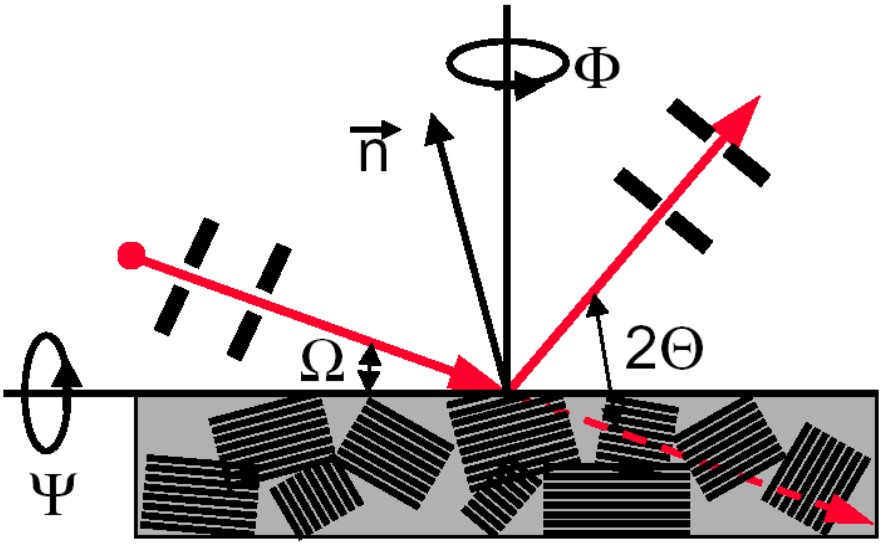

Figure 47. Schematic drawing of the orientation of crystallites in a polycrystalline sample, angle between incoming X-ray beam and sample surface Ω, scattering angle 2Θ, normal of the sample rotation Φ-axis and tilting of the sample Ψ. The orientation of the crystallite under investigation is described by its normal $\vec{n}$

The intensity of a Bragg reflection for an ideal powder, where the crystallites uniformly occupy all orientations in space, only depends on the scattering angle 2Θ but not on the rotation Φ or tilting Ψ of the sample (see chapter 5.1) (figure 47). In reality, the orientations of crystallites in polycrystalline material often produce anisotropic intensity distributions (textures) which can be visualized (pole figures) at constant 2Θ by rotating Φ and Ψ. Generally, the pole figures of at least 3 linear independent lattice planes (hkl) are required to quantitatively calculate the orientation distribution function (ODF) in 3-dimensional Euler space.

12.2 Stress

A typical pole figure of a sputtered Cu layer on silicon (100) substrate is given in figure 48. During sputtering, the Cu crystallites prefer to orient their close packed (111) planes parallel to the (100) plane of the silicon substrate. The texture influences material properties like conductivity. The texture in figure 48 is called fiber texture and shows a rotationally symmetric intensity distribution with respect to the surface normal with an intensity maximum at Ψ= 0°.

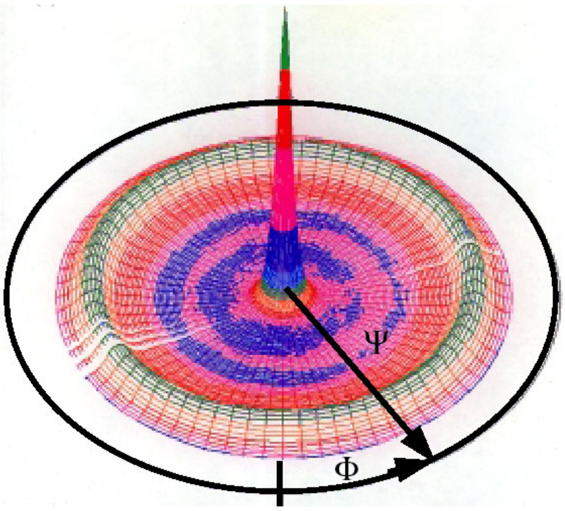

Figure 48. Pole figure of a sputtered Cu layer on silicon (100) substrate, showing a (111) fiber texture

To perform texture and (macroscopic) stress measurements (see below), the diffractometer must be equipped with an Eulerian cradle. The primary X-ray beam hits the sample and the reflected beam is then picked up via crossed soller slits so that the angular window within the pole figure is small enough in the plane of dispersion to enable good angular discrimination and is large enough in the vertical plane to collect as much intensity as possible. A typical setup is shown in figure 49.

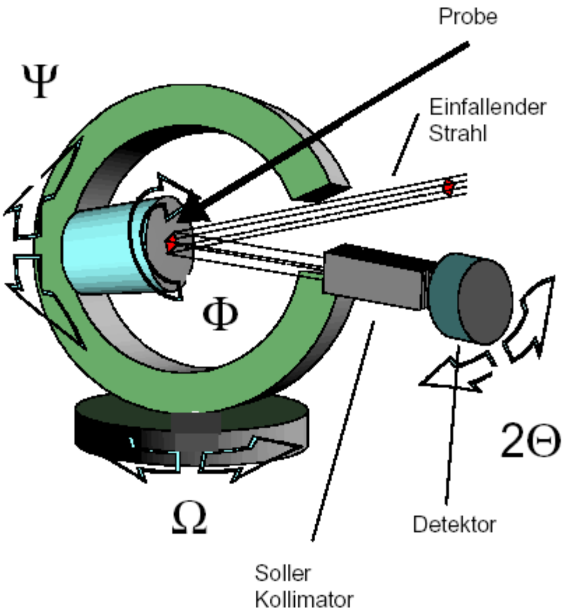

Figure 49 Diffractometer set up for texture and (macroscopic) stress measurements

X-ray powder diffraction is also a powerful method to analyze macroscopic stress in all directions in space by exact measurement of the d-spacing of a Bragg reflection (*hkl*) in dependence of the inclination of the lattice plane Ψ to the sample surface. In the case of a material under stress, the d-spacing is *not* independent of the orientation of the crystallites in the sample. When drawing the dilation ε=Δd/d in dependence of sin2Ψ, the slope m =

∂ε/∂(sin2(ψ)) reveals the stress direction and in combination with the elastic constants the amount of mechanical stress. The method has been used to study thermally induced stress in metals.

12.3 Microdiffraction

The detection of very small amounts of material plays an important role in mineralogy. With the availability of synchrotron radiation and image plate or CCD detectors, the detection limit of polymorphic phases is as low as 0.1 weight %. An exotic example, demonstrating the power of modern CCD technique in the laboratory is given in figure 50, where tiny grains of the secondary mineral vivianite, an iron-phosphate, could be identified in the skin of an ancient mummy found in the Austrian alps.

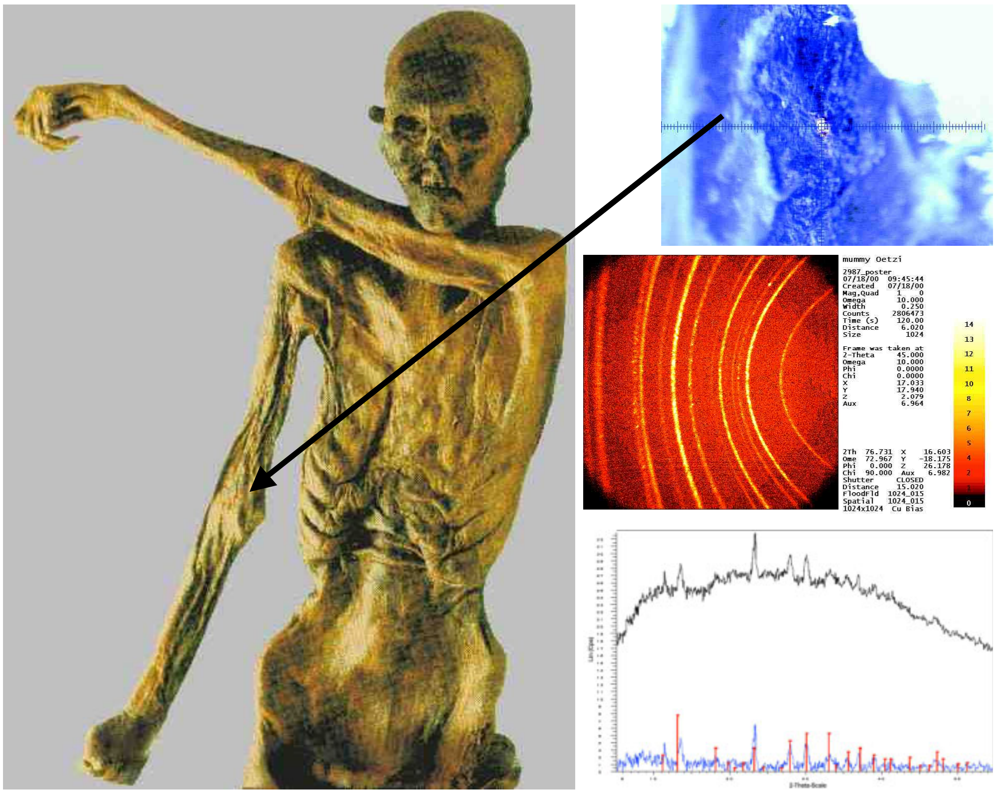

```
mummy Oetzi
2987_poster
07/18/00  09:45:44
Created   07/18/00
Mag,Quad   1    0
Omega       10.000
Width        0.250
Counts     2806473
Time (s)    120.00
Distance     6.020
Size          1024

Frame was taken at
2-Theta     45.000
Omega       10.000
Phi         0.0000
Chi         0.0000
X           17.033
Y           17.940
Z            2.079
Aux          6.964

2Th  76.731  X    16.603
Ome  72.967  Y   -18.175
Phi   0.000  Z    26.178
Chi  90.000  Aux   6.982
Shutter       CLOSED
Distance      15.020
FloodFld  1024_015
Spatial   1024_015
1024x1024  Cu Bias
```

Figure50: Tiny grains of vivianite (upper right) in the skin of the „Oetzi“ mummy (tyrolean mummified glacierman) (left) identified by X-ray microdiffraction using a laboratory CCD system (lower right)

13 Literature

Bish, D. L. & Post, J. E. (1989). Modern Powder Diffraction. Reviews in Mineralogy Vol. 20, Published by The Mineralogical Society of America, Washington, D.C., ISSN 0275-0279.

Bloss, F. D. (1971). Crystallography and crystal chemistry, Verlag Holt, Rinehart and Winston, New York [u.a.], ISBN/ISSN 0-03-085155-6, 545 S.

Brechbuehl, Kern, A., Jakob, R. Tessadri, 'Tiny grains of vivianite in the skin of the „Oetzi“ mummy, Denver X-ray conference 2000, collected abstracts.

David, W.I.F. (ed.) (2002) . Book about synchrotron powder diffraction.

Giacovazzo, C., Monaco, H. L., Viterbo, D., Scordari, F., Gilli, G., Zanotti, G. & Catti, M. (1992). *Fundamentals of Crystallography.* IUCr Texts on Crystallography 2. Ed. C. Giacovazzo. Oxford University Press, Walton Street, Oxford OX26DP. ISBN 0 19 855578 4.

International Tables for Crystallography, Volumes I-IV, published by the International Union of Crystallography by D. Reidel publishing company, Dordrecht: Holland/Boston, 1983.

Kern, A. (1992). Präzisionspulverdiffraktometrie: Ein Vergleich verschiedener Methoden. Diplomarbeit, Heidelberg, 175 S.

Kleber, W. (1983). *Einführung in die Kristallographie*, VEB Verlag Technik Berlin.

Klug, H.P. & Alexander, L.E. (1974). X-Ray Diffraction Procedures, 2nd Ed., J. Wiley and Sons Inc., New York, 996 pp.

Krischner, H. (1980). Einführung in die Röntgenfeinstrukturanalyse. Verlag Friedr. Vieweg & Sohn Braunschweig/ Wiesbaden, ISBN 3-528-18324-1.

McLachlan, D. (1957). *X-ray crystal structure,* McGraw-Hill Book Company, New York, Toronto, London.

Neder, R.B. & Proffen, Th. (1996). J. Appl. Cryst. 29, 727-735.

Schuster, M. (2001). Dünnschichtanalytik mit Röntgenmethoden, Report of Siemens AG, München.

Stutzman, P. E. & Leigh, S. (2000). NIST publication "Compositional Analysis of NIST Reference Material Clinker 8486". Cement Microscopy, 22nd International Conference. Proceedings. April 29-May 4, 2000, Montreal, Canada, 22-38.